Impact of physical parameterizations on wind simulation with WRF V3.9.1.1 under stable conditions at PBL gray-zone resolution: a case study over the coastal regions of North China ~~at PBL gray-zone resolution~~

Entao Yu[1,2], Rui Bai[1,3], Xia Chen[4,5], Lifang Shao[4]

[1] Nansen-Zhu International Research Centre, Institute of Atmospheric Physics, Chinese Academy of Sciences, Beijing, China
[2] Collaborative Innovation Center on Forecast and Evaluation of Meteorological Disasters (CIC-FEMD), Nanjing University of Information Science & Technology, Nanjing, China
[3] University of Chinese Academy of Science (UCAS), Beijing, China
[4] Hebei Climate Center, Shijiazhuang, China
[5] Hebei Key Laboratory for Meteorology and Eco-environment, Shijiazhuang, China

Correspondence to: Entao Yu (yuet@mail.iap.ac.cn) and Xia Chen (chenxia1218@sina.com)

Abstract. Reliable simulation of winds ~~patterns that form~~ under stable weather conditions is vital to prevent air pollution. Here, we investigate~~d~~ how different physical parameterization schemes impact simulated near-surface~~surface~~ wind at 10 meter height ~~simulations~~ over the coastal regions of North China using the Weather Research and Forecasting (WRF) model with a horizontal ~~resolution~~ grid spacing of 0.5 km. We perform~~ed~~ 640 ensemble simulations using multiple combinations of 10 planetary boundary layer (PBL), 16 microphysics (MP), and four shortwave-longwave~~/shortwave~~ radiation (S~~L~~W-~~/~~L~~S~~W) ~~radiation~~ schemes. Model performance ~~i~~was evaluated using measurements from weather station observations. The~~se data~~ results show that the WRF model can reproduce the temporal variation of wind speed in a reasonable way ~~and direction to a high degree of accuracy~~. The simulated wind speed is most sensitive to the PBL schemes, followed by S~~L~~W-~~/~~L~~S~~W radiation schemes and MP schemes~~, while wind direction is less sensitive to variation of the physical parameterizations~~. Among all PBL schemes, the MYJ scheme shows the strongest temporal correlation with the observed wind speed~~ation data~~, while the YSU scheme has~~d~~ the lowest~~smallest~~ model bias. ~~A combined~~ Dudhia~~ and~~ RRTM ~~scheme~~ and MYDM7 ~~scheme~~ show the best model performances out of all S~~L~~W-~~/~~L~~S~~W ~~radiation~~ and MP schemes, respectively~~. Our results show that t~~, the interactions among ~~physical components~~schemes also have large influence ~~play an important role in~~ on wind simulation~~s~~. Further investigation~~s~~ indicate that model sensitivity is also impacted by ocean proximity and elevation ~~land type has a profound influence on model sensitivity.~~ For example, for ~~the weather stations located in~~ the coastal stations~~regions~~,~~.~~ ~~The~~ MYNN ~~scheme~~ show~~sed~~ the ~~highest~~ best temporal correlation ~~among all PBL schemes, while LES and YSU has the smallest model errors among all PBL schemes~~, ~~the RRTMG and~~ while Goddard ~~schemes~~ show~~sed~~ ~~the highest correlations and smallest~~the smallest ~~biases~~ bias out of ~~all~~ S~~L~~W-~~/~~L~~S~~W ~~radiation~~ schemes, these results are different from that of inland stations. In general, WRF simulates wind speed less accurately for coastal stations compared to inland stations, and error metrics tend to degrade with

increasing elevation. The WRF model shows worse performance in reproducing the temporal variation of wind direction, with lower correlation coefficient compared to that of wind speed. Our results indicate the roles that various parameterization schemes play in wind simulations under stable weather conditions, and provide a valuable reference for further research in this region the study area and nearby regions and in other locations around the world.

1 Introduction

Megacities that experience rapid urbanization and economic development also commonly suffer from a simultaneous decline in air quality (Ulpiani, 2021). For example, numerous haze events have been reported in the Beijing, Tianjin, and Hebei regions of North China over the past few decades. Haze-related weather and associated high concentrations of fine particulate matter have negative impacts on public health and the environment (Wang and Mauzerall, 2006). These events can significantly disrupt economic growth, as demonstrated by the severe haze events that occurred over North China in January 2013 (Zhang et al., 2014; Zhang et al., 2015; Cai et al., 2017; Zhang et al., 2015). These events are most frequent in boreal winter and are closely related to local weather conditions, with haze forming in regions with low wind speeds (Li et al., 2015; Wang et al., 2021; Li et al., 2015). Projections of future climate change suggest that global temperatures will increase, and the frequency of conducive weather conditions to severe haze is projected to increase substantially in responds to the climate change, which in turn may increase the frequency of haze events over North China (Cai et al., 2017), however, numerical models always show large bias in wind prediction over China (Gao et al., 2016b; Zhao et al., 2016; Pan et al., 2021), Therefore, thus it is crucial to improve wind predictions of wind field behavior under stable weather conditions in order to minimize associated economic losses and environmental impacts.

In recent years, numerical models have been used extensively to study the weather and climate over China, as they have high spatial and temporal resolutions, and employ sophisticated physical parameterization schemes that can reproduce detailed atmospheric and land surface processes (Wang et al., 2011; Zhou et al., 2019; Kong et al., 2021; Zhou et al., 2019). However, these models mostly focus on temperature or precipitation, and only a few studies have attempted to simulate wind patterns over China (Li et al., 2019; Xia et al., 2019; Pan et al., 2021; Xia et al., 2019). FurthermoreMeanwhile, numerical models inherently involve many sources of uncertainty, as they cannot resolve all processes that occur in the real world; instead, parameterizations are needed to represent the effect of key physical processes, such as radiative transfer, turbulent mixing, and moist convection that occur at the sub-grid scaleradiative heating, planetary boundary layers, and cloud microphysics. Different physical parameterization packages schemes depictreproduce natural phenomena to different degrees of accuracy and choosing appropriate combinations is extremely important, as this decisionit strongly influences the model simulation results (Yu et al., 2011; Gómez-Navarro et al., 2015; Stegehuis et al., 2015; Gao et al., 2016b; Yang et al., 2017; Taraphdar et al., 2021; Gómez-Navarro et al., 2015; Stegehuis et al., 2015).

The impact of planetary boundary layer (PBL) schemes on wind simulations has been studied in recentfor many years, as PBL schemes play a critical role in modulating mass, energy, and moisture fluxes between the land and atmosphere, which in turn

influence the simulation of low-level temperatures, cloud formation, and wind fields (Jiménez and Dudhia, 2012; Gómez-Navarro et al., 2015; Gonçalves-Ageitos et al., 2015; Falasca et al., 2021; Gholami et al., 2021~~; Gómez-Navarro et al., 2015; Jiménez and Dudhia, 2012; Gonçalves-Ageitos et al., 2015~~). A lot of studies indicate overestimation of wind speed in WRF simulation with different PBL schemes (Jiménez and Dudhia, 2012; Carvalho et al., 2014a, b; Pan et al., 2021; Gholami et al., 2021; Dzebre and Adaramola, 2020), for example, Gómez-Navarro et al. (2015) investigated the sensitivity of the WRF model to PBL schemes by simulating wind storms over complex terrain at a horizontal ~~resolution~~ grid spacing of 2 km. In that study, the WRF model was ~~combined~~ configured with the Mellor-Yamada-Janjic (MYJ) scheme and overestimated wind speed by up to 100%, however, the~~ir~~is bias was significantly reduced when the non-local scheme developed at Yonsei University (YSU) was used instead, the YSU scheme also shows good model skill in simulating winds~~. Other studies conducted~~ over the northeastern Iberian Peninsula, Persian Gulf, Tyrrhenian coast, and western Argentina ~~produced similar results~~ (Jiménez and Dudhia, 2012; Puliafito et al., 2015; Falasca et al., 2021; ~~Jiménez and Dudhia, 2012; Puliafito et al., 2015;~~ Gholami et al., 2021)~~.~~ There are also ~~although~~ some studies suggesting ~~have suggested that the~~ MYNN and ACM2~~ schemes~~ are more appropriate for wind simulations (Carvalho et al., 2014b; Chang et al., 2015; Prieto-Herráez et al., 2021; Rybchuk et al., 2021~~; Chang et al., 2015; Carvalho et al., 2014b~~).

The performance of wind simulation is ~~performance of numerical models simulating wind patterns is~~ also affected by the choice of cloud microphysics (MP) parameterization~~s scheme~~. Cloud microphysical processes, such as moisture evaporation and condensation, can affect thermodynamic and dynamic interactions in the atmosphere (Rajeevan et al., 2010; Santos-Alamillos et al., 2013; ~~Rajeevan et al., 2010;~~ Li et al., 2020), ~~and so~~then affect the vertical distribution of heat and the ~~behavior of~~ wind fields close to the Earth's surface. ~~Recently,~~ Cheng et al. (2013) reported that predictions of summer wind speeds in northern Colorado were strongly affected by the choice of ~~cloud~~ MP parameterization scheme~~s., and that the WRF double moment 6-class (WDM6) scheme performed best.~~

Another factor ~~that influences the veracity of~~influencing wind simulation~~s~~ is the choice of radiation parameterization scheme~~s~~, which includes shortwave ~~(SW)~~ radiation and longwave ~~(LW)~~ radiation (SW-LW) schemes. Differences in surface radiation intensities can generate thermal contrasts in regions with complex topography, which in turn affect local and low-level wind distribution patterns (Santos-Alamillos et al., 2013).

The interactions among physical parameterizations are also vital to wind simulation, as they may alter the processes of atmosphere-land interactions, radiation transport, and moist convection, and amplify the uncertainties in wind prediction. The impact of parameterization combination on WRF performance has been investigated in previous studies (Santos-Alamillos et al., 2013; Fernández-González et al., 2018), Fernández-González et al. (2018) reported that there is no single combination of parameterizations that performs best during all weather conditions.

Most of the aforementioned studies ~~only~~ considered a small number of ~~combinations of physical~~ parameterization schemes, to the best of our knowledge, ~~meaning that~~ the sensitivity of ~~physical processes~~ parameterizations on ~~simulated wind patterns~~wind simulation has not ~~yet~~ been explored in a systematic way in China. In this study, we systematically evaluate the performance of a large number of parameterization combinations, including PBL, MP, and SW-LW schemes.~~Performing such an~~

~~investigation is important, as error compensation among processes that involve low-level atmosphere-land interactions, radiation, and clouds may predict incorrect wind distribution patterns. In this study, we systematically evaluated the performance of 640 combinations of physical parameterization schemes, including PBL, MP, and SW/LW radiation processes.~~

Th~~is was~~e investigation is conducted using the WRF model at ~~a very high resolution~~a grid spacing of 0.5 km, which belongs to the PBL "gray zone" resolution that is too fine to utilize mesoscale turbulence parameterizations and too coarse for a large-eddy-simulation (LES) scheme to resolve turbulent eddies (Shin and Hong, 2015; Honnert et al., 2016)~~for the PBL scale~~. Our main objective was to identify a set of ~~multi-physics~~ configurations of the WRF model that can best reproduce wind fields under stable weather conditions over North China, which experienced many winter haze events during the past a few years. This study addressed the following research themes: (1) quantify the sensitivity of wind simulation ~~simulated wind field under stable conditions~~ to different ~~physical~~ parameterization~~s schemes~~ under stable conditions, and (2) refine optimized configurations with the best performance in reproducing winds under stable conditions over North China~~refine an optimized model configuration of WRF model to reproduce the wind field~~. These results would provide valuable ~~insights into~~evaluation of WRF ~~model~~ performance, and be helpful in ~~can be used to produce more reliable and accurate~~ wind and air quality forecast~~ing~~ at the study area. The finding~~founding~~ reported here may also be ~~applied~~ informative to other regions around the world.

This paper is structured as follows: section 2 describes the model setup and the evaluation data, model results are reported in section 3, and discussion and concluding remarks are given in section 4 and 5.

2. ~~Description of the study area, model, and experimental design~~Data and methods

2.1. ~~Study area and stable weather events in 2019~~ The stable weather event in 2019

The study area is located in the central section of the "Bohai Economic Rim", which is bordered to the southeast by the Bohai Sea and to the northwest by the Yan Mountains (Figure 1a). This region traditionally hosts heavy industry and manufacturing businesses, and is a significant region of economic growth and development in North China (Song et al., 2020; Zhao et al., 2020). Air quality in this area has declined over the past ~~few~~ decades, and the frequency of winter haze events has increased due to increased pollutant emissions and favorable stable weather conditions with lower wind speed (Gao et al., 2016a; Cai et al., 2017). For instance, during the heavy fog and haze event~~severe haze events~~ over eastern China in January 2013, an anomalous southerly wind in the lower troposphere caused by the weak East Asian winter monsoon weakened the synoptic ~~disturbances~~ forcing and extent of vertical mixing in the atmosphere, thus increas~~ed~~ing the stability of ~~surface~~ air in the boundary layer and ~~favoring~~ the local concentration of hazes (Zhang et al., 2014).

~~A severe haze event occurred in the study area during January 11th to January 15th, 2019. At this time, the peak PM2.5 and PM10 concentrations measured in Tangshan city, located in the center of the study region, exceeded 279 μg/m3 and 357 μg/m3, respectively. The haze event also occurred under stable weather conditions with an average wind speed lower than 5 m/s (Figure 2a). The wind rose for this event showed a primarily southerly wind at the surface (Figure 2b), indicating a weakened~~

~~East Asia winter monsoon and stable lower troposphere. This event was used to evaluate the performance of the physical parameters of the WRF model, as shown below.~~

During 11-15 January 2019, a severe haze event occurred in the study area, the peak PM2.5 and PM10 concentrations exceeded 279 μg/m3 and 357 μg/m3 in TangShan city, and 282 μg/m3 and 358 μg/m3 in QinHuangDao city, respectively, the locations of the two cities can be found in Figure 1. Figure 2 depicts the distribution of geopotential height, winds, and cloud fraction during the study period, the geopotential height and winds data are from the ERA5 dataset (Hersbach et al., 2020), and the cloud fractions are from satellite observations of CLARA (CM SAF cLoud, Albedo and surface Radiation) product family (Karlsson et al., 2021). Figure 2 indicates that a weak high-pressure system persisted from 11 to 13 January, along with weak southwest wind in the study area, which would transport warm and wet air to the study area (Gao et al., 2016a), creating a favorable moisture condition for stable conditions and inhibiting pollutants dispersal (Zhang et al., 2014; Hua and Wu, 2022). Then the high-pressure system was replaced by strong northwest wind from 14 to 15 January 2019. The CLARA observations indicate cloud fraction exceeding 60% on 12 January at the study area, while for the rest of the time, cloud fraction is low. This stable event is used to investigate the impact of physical parameterizations of the WRF model.

2.2 ~~WRF m~~Model configurations

WRF model (version 3.9.1.1) with an advanced research WRF (ARW) core is~~was~~ used in this study, which is a non-hydrostatic atmospheric model with terrain-following vertical coordinates (Skamarock et al., 2008). The simulations contain~~ed~~ three one-way nested domains with horizontal ~~resolutions~~ grid spacing of 8 km, 2 km, and 0.5 km for D01, D02, and D03, respectively (Figure 1b). The computational domains ~~were~~ are based on a Lambert conformal conic projection centered at 38.5°N and 120°E, with 360 × 480, 381 × 381, and 341 × 421 grid points for D01, D02, and D03, respectively. The ~~following analysis evaluates model performance~~evaluations are based on the innermost domain, which covers the coastal and surrounding regions of North China (Figure 1a). ~~This~~ The simulation domain has~~d~~ 65 vertical levels, and the eta values for the first 10 levels are 0.996, 0.988, 0.978, 0.966, 0.956, 0.946, 0.933, 0.923, 0.912, and 0.901, ~~which~~this ensure~~sd~~ that sufficient model~~several~~ levels exist~~ed below~~ within the PBL ~~height~~ at any time.

The ERA5 reanalysis dataset, which has a horizontal resolution of 0.25° and 38 vertical levels, ~~and was~~is used ~~as to define~~to provide the initial and boundary conditions for ~~all~~ WRF simulations. The WRF model ~~was~~is initialized at 00:00 UTC (08:00 local time) 9 January ~~9th,~~ 2019 ~~and integrated until 00:00 UTC January 16th, 2019~~, with the first 40 hours treated as the~~a~~ spin-up period. Firstly, the d~~D~~efault physical parameterization schemes (Table 2) ~~were~~ are applied in the single set of WRF ~~model~~ simulations for the outer two domains (D01 and D02), and then the output ~~from these domains~~of D02 ~~was~~ is used to drive inner domain simulations with different combinations of PBL, MP, and SW ~~/~~LW ~~radiation parameterization~~ schemes (see section 2.3). This approach helps~~ed~~ to isolate the impacts of parameterization within the inner domain from changes in boundary forcing (Yang et al., 2017). All the simulations applied the Noah land surface model with multi-parameterization options (Noah-MP, Yang et al., 2011; Niu et al., 2011.)~~No other parameterizations were changed in any of the other simulations, including the Noah-MP land surface scheme (Yang et al., 2011; Niu et al., 2011).~~ The lateral boundary conditions and sea

surface temperature are~~were~~ updated every three hours using the ERA5 reanalysis data, and the ~~modeled frequency of wind was calculated hourly~~ frequency of wind retrieved from WRF output is hourly, which matches the frequency of observations in the study area.

2.3 Experimental design

The WRF model contains different ~~components~~ parameterization schemes that represent different physical processes ~~(e.g. PBL, MP, and LW/SW radiation)~~. Further, every ~~physical process~~ scheme in the model has many parameters, such that a model can range from being simple and efficient to sophisticated and computationally costly. In this study, a systematic evaluation of parameterizations ~~A comprehensive test of all parameterization schemes was~~ is achieved by considering 10 PBL ~~schemes~~, 16 MP ~~schemes~~, and four LW~~-~~/SW ~~radiation~~ schemes, which produce~~d~~ 640 (i.e., 10 × 16 × 4) combinations in total~~a total of 640 (i.e. 10 × 16 × 4) combinations that were investigated in this study~~.

The ~~PBL~~ parameterization schemes investigated in this study are listed in Table 1. As ~~T~~the horizontal ~~resolution~~ grid spacing of 0.5 km is within the PBL "gray zone~~"~~ ~~grid spacing~~resolution ~~that is too fine to utilize mesoscale turbulence parameterizations and too coarse for a large-eddy simulation (LES) scheme to resolve turbulent eddies; therefore~~, both PBL and LES assumptions are imperfect ~~at this resolution. In this study~~, we test both PBL and LES schemes in this study ~~were tested~~. For the LES configuration, the~~a~~ 1.5-order turbulence kinetic energy closure model ~~was~~ is used to parameterize motion at the sub-grid scale (Deardorff, 1985). For the YSU scheme, ~~a~~ topographic correction for surface winds ~~was~~ is included to represent extra drag from sub-grid topography and enhanced flow at hill tops (Jiménez and Dudhia, 2012). The option for top-down mixing driven by radiative cooling ~~was~~ is also turned on during the integration. For the rest of the PBL schemes, the default configurations ~~were~~ are chosen. The atmospheric surface layer (SL) is the lowest part of the atmospheric boundary layer~~. Calculated friction velocities and exchange coefficients within this SL were~~, of which the parameterizations are used to quantify surface heat and moisture fluxes in land surface model and ~~LSM schemes, alongside~~ surface stress in the PBL scheme~~s~~. In the current generation of ~~models~~WRF, the SL ~~options~~ schemes are tied to the PBL ~~options~~schemes. ~~Consequently, the~~ In this study, ETA, QNSE, MYNN, Pleim-Xiu, and TEMF ~~SL~~ schemes were chosen separately for PBL schemes of ~~the~~ MYJ, QNSE, MYNN, ACM2, and TEMF ~~PBL schemes~~. The revised MM5 scheme (Jimenez et al., 2012) was used for all other PBL schemes.

Sixteen MP schemes were applied in this study (Table 1), Lin, WSM3, WSM5, ETA, WSM6, Goddard, SBU, and NSSL1 schemes are the single-moment bulk microphysical scheme, which predicts only the mixing ratios of hydrometeors (i.e., cloud ice, snow, graupel, rain, and cloud water) by assuming particle size distributions. The other eight schemes (Thompson, MYDM7, Morrison, CMA, WDM6, NSSL2, ThompsonAA and P3) use a double-moment approach, predicting not only mixing ratios of hydrometeors but also number concentrations. Among them, two types of hydrometeors are included in WSM3 (cloud water and rain), three types of hydrometeors are included in ETA (cloud water, rain, and snow) and P3 (cloud water, rain, and ice), four types of hydrometeors are included in WSM5 and SBU (cloud water, rain, ice, and snow), five types of hydrometeors are included in Lin, WSM6, Goddard, Thompson, Morrison, CAM, WDM6 and ThompsonAA (cloud water, rain, ice, snow, and graupel), six types of hydrometeors are included in MYDM7, NSSL1, and NSSL2 (cloud water, rain, ice,

snow, graupel, and hail). According to the user's guide of ARW (Skamarock et al., 2008), WSM6, Thompson, Morrison, WDM6, NSSL1, and NSSL2 are suitable for high-resolution simulations. ~~Sixteen MP schemes were used in this study, as documented in Table 2. Lin scheme is a sophisticated scheme suitable for high-resolution simulations of real data. The WSM3, WSM5, WSM6, and WDM6 schemes share a similar underlying theory, and WSM6 and WDM6 are suitable for high-resolution simulations. The ETA scheme represents the operational microphysics behavior in NCEP models. Goddard, Thompson, Morrison, NSSL2, and NSSL1 are new schemes suitable for high-resolution simulations. The MYDM7 scheme includes separate categories for hail and graupel, and models double-moment clouds, rain, ice, snow, graupel, and hail. Finally, CAM is a double moment 5-class scheme, and ThompsonAA considers water- and ice-friendly aerosols.~~

Four SW-LW combinations are applied in this study (Table 1), ~~were selected for LW/SW radiation schemes.~~ Dudhia is a simple and efficient shortwave radiation scheme for clouds and clear-sky absorption and scattering; ~~the~~ RRTM ~~scheme~~ provides accurate and efficient look-up tables for longwave radiation; ~~and the~~ CAM SW-LW scheme~~s~~ are~~is~~ derived from the CAM3 ~~climate~~ model used in CCSM3, and allows modeling of aerosols and trace gases. ~~Finally,~~ RRTMG is a new ~~LW/SW~~ scheme~~s~~ that utilizes a Monte Carlo independent column approximation (MCICA) method of random cloud overlap.

2.4 Observational data and evaluation metrics

Observations from weather stations across the study region ~~were~~ are used to evaluate the performance of the model. These stations are operated by the China Meteorology Administration (CMA), and report wind speed and direction at an altitude of 10 m. In this study, we use~~d~~ two-minute-averaged wind speed at hourly frequency. All data ~~that were collected were~~ are screened before analysis in order to remove stations with data showing spurious jumps (e.g., wind speed jumps to 0 m/s due to frozen sensor). After this filtering, 105 out of 132 weather stations (Figure 1a) are remained, including 89 inland stations and 16 coastal stations~~.~~ The results of WRF ~~simulations were~~ are directly compared with observations made at each weather station, which ~~was~~ is achieved by using the model result that ~~was~~ is geographically closest to the weather station under consideration. Although some errors are introduced when performing these comparisons, they are systematic and shared by all simulations, and therefore have minor effects on the evaluation of model performances.

Several metrics ~~were~~ are employed for evaluating the performance of each model configuration, including the Pearson's correlation coefficient (CORR), BIAS, root mean square error (RMSE), and the Taylor skill score (T). They~~se~~ are defined as follows:

$$CORR = \frac{\sum_{i=1}^{N}(M_i-\overline{M})(O_i-\overline{O})}{\sqrt{\sum_{i=1}^{N}(M_i-\overline{M})^2 \cdot \sum_{i=1}^{N}(O_i-\overline{O})^2}}$$

$$BIAS = \frac{1}{N}\sum_{i=1}^{N}(M_i - O_i)$$

$$RMSE = \sqrt{\frac{1}{N}\sum_{i=1}^{N}(M_i - O_i)^2}$$

$$T = \frac{2(1+CORR)}{\left(SD+\frac{1}{SD}\right)^2}$$

$$CORR = \frac{\sum(m_t - \overline{m}) \cdot \sum(o_t - \overline{o})}{\sqrt{\sum(m_t - \overline{m})^2 \cdot \sum(o_t - \overline{o})^2}}$$

$$BIAS = \sum(m_t - o_t)$$

$$RMSE = \sqrt{\frac{\sum(m_t - o_t)^2}{N_t}}$$

$$T = \frac{2(1 + CORR)}{\left(SD + \frac{1}{SD}\right)^2}$$

Here, Mm_t is the value of the model output, Oo_t is the value of the observation, NN_t is the number of observations, and SD is the ratio of simulated to observed standard deviations. The Higher Taylor skill score ranges from zero to one, and a higher score indicates a more accurate simulation (Gan et al., 2019).

The difference in wind direction was calculated as follows:

$$\Delta = \begin{cases} M - O, \ when \ |M - O| \leq 180° \\ (M - O)(1 - \frac{360}{|M-O|}), \ when \ |M - O| > 180° \end{cases}$$

$$\Delta = \begin{cases} m - o, \ when \ |m - o| < 180° \\ (m - o)(1 - \frac{360}{|m-o|}), \ when \ |m - o| > 180° \end{cases}$$

The correlation between simulated and measured angles is was determined by a circular correlation coefficient (CORR), and the mean of angular is calculated using vector notation approach, circular correlation coefficient i which was calculated as follows:

$$CORR = \frac{\sum_{i=1}^{N} sin(\alpha_i - \overline{\alpha}) sin(\beta_i - \overline{\beta})}{\sqrt{\sum_{i=1}^{N} sin^2(\alpha_i - \overline{\alpha}) sin^2(\beta_i - \overline{\beta})}}$$

$$CORR = \frac{\sum \sin(\alpha - \bar{\alpha}) \sin(\beta - \bar{\beta})}{\sqrt{sin^2(\alpha - \bar{\alpha}) sin^2(\beta - \bar{\beta})}}$$

Here, α and β are simulated and observed wind direction angles, respectively.

3. Results

~~Simulated wind speeds and directions were compared with observations recorded by CMA weather stations. The comparison presented here is based on the average of all 1056 weather stations, which provides general evaluation of the model performance when using different physical parameterization schemes. The section below first analyzes the impact of physical parameterization schemes, and then investigates the effects of topography and land type.~~

3.1 ~~Sensitivity to~~Impacts of physical parameterizations on wind speed and direction simulations ~~schemes~~

3.1.1 ~~Impact of~~ PBL ~~parameterizations~~

Figure 3a shows the time series of observed wind speeds in local time and the corresponding simulations~~simulated data produced by~~ using different PBL schemes. The WRF model ~~closely~~ generally reproduces the temporal variation of observed wind speed in the study area with exaggeration; in particular, the shift from low to high ~~values recorded~~wind speed on 14 January ~~14th,~~ 2019~~,~~ is reproduced by all schemes except for QNSE, with which the wind speed change is considerably larger than with all other schemes ~~showed no obvious daily wind speed change~~ during the simulation period. ~~Despite this correlation, simulations generally overestimated the wind speed, with absolute differences exceeding 10 m/s.~~ Almost all the PBL schemes overestimate wind speed by 1 m/s, however, for the QNSE scheme, the largest overestimation exceeding 10 m/s during daytime on 11 and 15 January 2019. ~~The overestimation of wind speed in such models has been widely reported by previous studies performed in other locations and using various WRF configurations (Jiménez and Dudhia, 2012; Carvalho et al., 2014a, b; Pan et al., 2021; Gholami et al., 2021; Dzebre and Adaramola, 2020). The QNSE scheme is a clear outlier by having model results that deviate significantly from observation data. This indicates that the scheme fails to reproduce reasonable wind speeds, although the other nine PBL schemes performed much better to similar degrees.~~ Further comparison shows that the difference between simulation and observation is lower during 11-13 January 2019 with the LES scheme, while YSU shows lower difference during 14-15 January 2019.~~indicates that model BIAS value was relatively smaller for LES configurations during the first three days of simulation time, while YSU showed a smaller BIAS value during the final two days of the simulation. The differences among different PBL schemes were relatively large in January 15th, 2019~~ In addition, the spread within the PBL schemes is larger on 15 January 2019, partly due to high~~faster observed~~ wind speed~~s~~ (> 4 m/s) or the general error growth in the model.

The statistics of CORR, BIAS and RMSE are illustrated in Figure 3b-d, MYJ shows the best CORR score of 0.96, MYNN, ACM2 and UW are slightly worse according to this verification score. YSU is the best scheme in term of BIAS and RMSE with the scores of 0.45 m/s and 0.61 m/s, flowed by MYNN (0.55 m/s and 0.70 m/s). The ranges of statistic scores across the 105 stations are also illustrated in Figure 3, for the schemes except QNSE, the range of CORR is 0.2-0.8, the range of BIAS is -2-2 m/s, and the range of RMSE is 0.7-2.5 m/s. Further comparison indicates that the CORR scores for individual station are lower than the average, while the BIAS and RMSE scores are higher than the average. For the QNSE scheme, the maximum BIAS and RMSE scores for individual station exceed 10 m/s and 16 m/s, indicating that it has problem in reproducing wind

speed under stable conditions over the study area. ~~Table 4 shows statistics for wind speed data calculated for different PBL schemes. In each case, bold and underlined data represent the highest CORR values, the smallest BIAS values, and the smallest RMSE values.~~ ~~WRF configurations that used the MYJ scheme showed the strongest correlations with observed data (0.956), followed by those that used MYNN, ACM2, UW, YSU, and the Shin-Hong schemes (>0.93). However, evaluation of model errors showed that the YSU scheme had a BIAS of 0.448 m/s and RMSE of 1.585 m/s, showing that it performed best out of all combinations. Simulations performed with the MYNN scheme show similar statistics to those with the YSU scheme. For the QNSE scheme, the extremely low CORR value (0.643) and high degree of error (BIAS = 3.218 and RMSE = 4.839) indicates that the scheme is not useful to model stable weather conditions in the study area. Its failure to reproduce wind speed data may be related to the eddy diffusivity mass-flux method used by QNSE during the daytime, which produces unrealistically fast wind speeds when compared with observed values (Figure 3). As such, all simulations using the QNSE scheme (64 simulations in total) were omitted from further investigation in order that these anomalous data did not affect our overall analysis.~~

~~Figure 4 presents a wind rose showing observed and simulated data produced via different PBL schemes. The simulated wind directions were very similar in all schemes, indicating that it is insensitive to changes in physical parameterizations; however, the main wind direction observed during this period was south, while the simulations primarily showed a southwesterly wind, suggesting that almost all PBL schemes have a clockwise bias in the modeled wind direction. As the simulated wind direction was calculated using the wind speed, the bias in modeled wind direction can be attributed to bias in the wind speed simulation.~~ Figure 4 shows the wind roses during 11-15 January 2019 from observation and simulations with different PBL schemes, as well as the statistic scores. Observations indicate that during the study period, wind is mostly from southwest to northwest direction (225-330°), while simulations with different PBL schemes produce primarily southwest wind (200-270°), indicating an anticlockwise bias of wind direction over the study area under stable conditions. Further comparison indicates that all PBL schemes strongly overestimate the speed of north wind compared to the observations, which is the main cause of positive bias in wind speed (Figure 3). The CORR scores of wind direction (0.42-0.59) are notably lower than that of wind speed, indicating degraded performance of WRF in wind direction simulation. LES shows the best CORR score of 0.59, while TEMF shows the best BIAS and RMSE scores of -11° and 56°. ~~Table 5 shows statistics for wind direction determined for different PBL schemes. Correlation coefficients for wind direction are generally lower than those for wind speed. The WRF configuration using the BouLac scheme shows the highest value of CORR (0.488), and LES simulations have the smallest RMSE values. As mentioned previously, the simulated wind directions are not sensitive to the physical schemes chosen. Consequently, the model RMSE and BIAS values for different PBL schemes are similar, and so the following analysis mainly focuses on the wind speed simulations.~~Considering the large model bias in wind speed, simulations with the QNSE scheme (64 in total) are omitted from further investigation in order that these anomalous data do not affect our overall analysis.

3.1.2 MP ~~Impact of microphysics parameterization~~

Figure 5 shows the time series of wind speed from the observation and simulations ~~observed wind speeds and simulated data produced using~~ with different MP schemes. The simulations are ~~Data from these simulations are~~ similar, especially during 14-15 January 2019~~the latter parts of the analysis period~~. The spread among simulations with different MP schemes is ~~of simulation data is~~ smaller than that with ~~shown by the~~ different PBL schemes, indicating that wind speed is less sensitive to the MP schemes~~. have a smaller influence on surface wind speed. Nonetheless, some differences still exist among the MP schemes.~~ The CORR scores are generally the same for all the MP schemes, while MYDM7 is the best scheme according to BIAS and RMSE scores, followed by P3 and ETA. The range of statistic scores across the stations are similar among the simulations with different MP schemes, which provides a further indication of low sensitivity of wind speed to MP schemes. ~~Statistics indicate that WRF configurations using the MYDM7 scheme show the highest CORR values (0.944), smallest BIAS values (0.660 m/s), and smallest RMSE values (1.788 m/s) when compared with observed wind speeds (Table 6). As such, this scheme showed the best model performance for wind speed simulation. Simulations performed with the ETA, Goddard, NSSL1, Thompson, P2, and Lin schemes show CORR values that are similar to MYDM7, and simulations performed with the P3, NSSL1, and ETA schemes have BIAS values that are slightly higher than that for MYDM7.~~

The sensitivity of wind direction to the MP schemes is also low, as the wind roses from simulations with different MP schemes are very similar (Figure 6). WDM6, NSSL2 and ThompsonAA show the best CORR score of 0.52, followed by Thompson and CAM5. Meanwhile, WSM3 is the best scheme according to the BIAS score, and ThompsonAA is the best scheme according to the RMSE score. ~~Simulated wind directions were similar in all cases, and models using the Goddard scheme showed the highest CORR values. By contrast, WRF configurations using the MYDM7 scheme had the smallest model error (i.e., BIAS and RMSE values).~~

3.1.3 Radiation~~Impact of radiation parameterization~~

Figure ~~6~~ 7 shows the time series of observed and simulated wind speeds, the ensemble spread among different SW-LW schemes is larger than that with different MP schemes, but smaller than that with different PBL schemes, which indicates that simulated wind speed is ~~and simulated data, where it can be seen that simulated wind speeds are~~ more sensitive to the SW-LW schemes ~~LW/SW radiation parameters~~ than the MP schemes, and less sensitive to the PBL schemes.~~. The LW/SW schemes have a larger model spread, but are still less sensitive than PBL schemes~~. Further comparison indicates that ~~Simulations with the~~ RRTMG and CAM show strong overestimation of ~~schemes overestimated the~~ wind speed, especially for the peak values during the daytime. Simulations with the Dudhia-RRTM schemes ~~Conversely, the WRF configurations using the Dudhia and RRTM schemes substantially~~ reduce the bias to a certain extent~~d this overestimation~~, and are ~~thus produced values that were much~~ closer to ~~weather~~ the station observations. The CORR scores are the same for the SW-LW schemes, and Dudhia-RRTM is the best scheme according to BIAS and RMSE scores, followed by Goddard.

Figure 8 shows the wind roses during 11-15 January 2019 from simulations with different SW-LW schemes and the corresponding statistic scores. The simulations indicate the wind is mostly form southwest direction during the study period, which is different from the observation. According to the CORR score, Dudhia-RRTM is the best scheme with the highest value (0.55), meanwhile, RRTMG shows the best BIAS score of -16°, and Dudhia-RRTM shows the best RMSE score of 61°. ~~Table 7 lists wind speed and wind direction statistics for these models. For simulated wind speeds, the Dudhia and RRTM schemes produced the best model results, as defined by having the highest CORR values (0.943), the smallest BIAS values (0.646 m/s), and smallest RMSE values (1.754 m/s). Simulations that employed the Goddard scheme produced similar wind speeds. For simulated wind directions, WRF configurations that used the CAM scheme had the highest CORR and lowest RMSE values, while simulations that employed the RRTMG scheme showed the lowest BIAS values.~~

3.1.4 ~~Impact of physical components i~~Interactions among physical parameterization schemes

Interactions among physical parameterizations~~components~~ also play an important role in wind simulation~~s~~. Since it is not possible to show ~~or discuss~~ all possible combinations of PBL, MP, and SW-LW ~~LW/SW radiation~~ schemes in this study, the results of interactions between PBL and SW-LW ~~LW/SW radiation~~ schemes are ~~used~~ selected as an example, which is illustrated in (Figure ~~7~~9). ~~All simulations shown in Figure 7 employed MYDM7 as t~~The MP schemes applied in the simulations are MYDM7 and P3, given that ~~it recorded~~ they show ~~the best~~ better performance in earlier ~~examples~~investigations (see S~~s~~ection 3.1.2). ~~. A total of 40 simulations were~~ thus for each MP scheme, a total of 36 simulations (excluding QNSE) are evaluated ~~in this way, which produced outcomes that were fully consistent with other results~~and the results are expected to be consistent with evaluations using other MP schemes. For wind speed simulation with both MYDM7 and P3,~~s, as illustrated in previous analyses, WRF configurations that used the~~ MYJ ~~scheme~~ show~~ed~~ the ~~highest~~ best CORR score~~values~~, while YSU shows the lowest BIAS and RMSE scores ~~and the YSU scheme produced the smallest model errors (Table 4)~~. However, ~~deeper~~ further investigation indicates ~~showed~~ that ~~the~~ YSU ~~scheme produced~~ shows lower BIAS and RMSE ~~values~~scores ~~only~~ when combined with Dudhia-RRTM or Goddard ~~the Dudhia and RRTM schemes together, or the Goddard scheme by itself. W~~,when it ~~was~~ is ~~combined~~ applied with ~~the~~ RRTMG ~~scheme~~, the BIAS and RMSE scores show obvious increasement compared with that with Dudhia-RRTM. ~~simulation errors were larger than those for the MYNN and combined Dudhia and RRTM schemes.~~ For the wind direction simulation, LES combined with Dudhia-RRTM shows the best CORR score, while TEMF is the best scheme according to BIAS and RMSE scores. ~~-~~Thus, the choice of suitable scheme combination also plays an important role in determining the model performance in the simulation of wind speed and direction. Overall, for BIAS and RMSE scores of wind speed, within each SW-LW group, the same PBL scheme ranks best (e.g., for wind-speed RMSE, no matter which PBL scheme, Dudhia-RRTM and Goddard are always best), and within each PBL scheme, the same SW-LW group ranks best, this indicates that a systematic variation of parameterizations is not necessary. However, for wind-speed CORR and wind direction, this pattern is not always consistent. For example, for wind-direction BIAS, the best SW-LW group depends on the choice of PBL scheme (e.g., for MYDM7 with TEMF, Dudhia-RRTM is best; for P3 MP scheme with TEMF, RRTMG is best), this indicates that a systematic variation of parameterizations is important when focusing on these variables. ~~for each physical~~

~~scheme, the choice of a suitable combination of related physical components is equally important to optimize model performance. These data show that simulations conducted using schemes with high correlation coefficients for PBL (MYJ), MP (MYDM7), and LW/SW radiation (Dudhia and RRTM) were not necessarily the same ones that had the highest individual values of CORR in all other simulations. The same result can be seen for wind direction simulations (Figure 7).~~

3.1.5 ~~Evaluation of model~~ WRF configurations with the best individual performance

To determine the WRF configuration with the best individual performance, Taylor skill scores are calculated for wind speed within all ~~-~~simulations, ~~for wind speed were calculated for all simulations.~~ The scores range from 0.2 to 1.0, with the best 10 WRF configurations having similar scores about 1.0.~~The statistics for the 10 best WRF configurations that showed the highest skill scores are listed in Table 8.~~ The timeseries and statistics are illustrated in Figure 10. The best 10 configurations have in common that they use the same PBL and SW-LW schemes, namely YSU and Dudhia-RRTM. Due to the slight differences between models using different MP schemes, the 10 best performing WRF configuration only vary in MP schemes~~The PBL and LW/SW radiation schemes used in this set were YSU and a combination of Dudhia and RRTM, respectively~~. This indicates ~~the significant influence~~ large impact of PBL and ~~radiation schemes~~ SW-LW on wind speed simulation~~s when~~ compared with MP ~~the MP schemes~~, and highlights ~~the better model~~ good performance of YSU and Dudhia-RRTM~~them both~~. ~~Because the~~ Since Taylor skill score considers both correlation (CORR) and stand deviation (SD), the best scheme (i.e., WDM6) ~~with the highest Taylor skill score value (i.e., WDM6)~~ is not the scheme that ~~had the highest~~ has the best CORR (i.e., Goddard), BIAS (i.e., MYDM7 and ETA), or RMSE (Goddard, NSSL1,MYDM7 and ETA). ~~value, lowest BIAS value, or lowest RMSE value. Indeed~~In fact, there ~~was~~ is no scheme that have all the best scores of CORR, BIAS and RMSE~~d both the highest CORR value and lowest model error (i.e., BIAS and RMSE values)~~. Thus, model ensemble ~~simulations are~~is needed to improve to ~~model~~ performance~~, although the number of members used in the ensemble also plays an important role in the determining its performance~~. Figure 10 ~~Table 8~~ also illustrates ~~list the statistics of~~ the ensemble ~~means~~ of different number of ~~the top two, three, four, five, seven, and 10~~ simulations, as well as a super ensemble of all the simulations (excluding ~~the~~ QNSE ~~scheme~~). The~~se~~ result indicates that ensemble mean of four simulations with WDM6, Goddard, NSSL1 and MYDM7 shows the lowest BIAS and RMSE scores.~~s show that the ensemble mean of the top four schemes (WDM6, Goddard, MYDM7, and NSSL1) performs best and has the smallest model error.~~ ~~Figure 8 shows a~~ Figure 10a shows the time series ~~for wind speed determined by the ensemble mean of the top four schemes, which was compared against data for all simulations.~~of wind speed from ensemble of 4 (ENS4) and all simulations (ENSall), the spread of ENS4 is significantly lower than ENSall, and ENS4 shows smaller difference with the observation compared to ENSall. ~~The general simulations show a large spread, whereas the ensemble mean of the top four schemes reduced the model bias.~~ Additionally, From the statistic scores we can find that ~~the ensemble of the top configurations~~ENS4 reduces model bias by approximately half compared to ENSall.~~, while its CORR value was highest of all the simulations.~~ ~~Figure 8 shows a time series for wind speed determined by the ensemble mean of the top four schemes, which was compared against data for all simulations. The general simulations show a large spread, whereas the ensemble mean of the top four schemes reduced the model bias.~~

3.2 Performance dependency on ~~land type~~ ocean proximity and elevation ~~and topography~~

Land surface conditions ~~(e.g., land–sea type or topography)~~ can affect the partitioning of sensible and latent heat fluxes, which ~~therefore~~ impacts local low-level circulation patterns and the wind distribution in a region (Yu et al., 2013; Barlage et al., 2016). The weather stations in the study region were classified into different groups according to their underlying surface type and topography. The effects of these parameters on the model results are presented below.

3.2.1 Ocean proximity~~Comparison between coastal and inland stations~~

Figure 11~~9~~ compares the results of wind speed for ~~simulations performed at~~ coastal stations (closer than 5 km from the shoreline, 89 stations in total) and inland stations (over 5km from the shoreline, 16 stations in total),~~ T~~the locations of these stations are shown in Figure 1a. For both coastal and inland stations, the ensemble spread is largest among the PBL schemes, followed by SW-LW and MP schemes~~Simulations from all stations indicate that modeled wind speed is most sensitive to the PBL scheme chosen, followed by LW/SW radiation and MP schemes~~, which is consistent with the results of previous analysies in this study. ~~The WRF model commonly~~WRF ~~overestimates wind speed at both coastal and inland stations~~reproduces the timeseries of wind speed reasonably, with larger overestimation for inland stations~~, and generally by the same magnitude. All simulations could reproduce the temporal variations of wind speed during the simulation period; however, the model spread was~~ Further comparison indicates that the ensemble spread is ~~relatively~~ larger for coastal stations compared to inland stations, especially among the MP schemes during 11-13 January 2019 with ~~for the first three days of the simulation period that exhibited~~ lower wind speed~~s~~. As such, in addition to physical parameterizations, model performance is also influenced by ocean proximity, and WRF simulates wind speed less accurately for coastal stations compared to inland stations. ~~land–sea interactions represent another source of model uncertainty, which generates greater model differences in wind simulations performed under stable weather conditions.~~

~~Table 9 presents statistics for simulations that considered differences between coastal and inland stations. One notable result is that~~The statistic scores are also illustrated in Figure 11, ~~the~~ CORR scores~~values~~ are consistently lower ~~for coastal stations are consistently lower than those for inland stations~~ and the BIAS and RMSE scores are generally worse for coastal stations compared to inland stations~~. Additionally, as there are no clear differences in wind speed values and variations, the difference in these CORR values~~, which indicates degraded ~~that~~ model performance ~~s are generally less reliable over coastal regions~~for coastal stations. This degradation may be caused by the uncertainties from the prescribed SST in our simulation, which may require better description of atmosphere-ocean coupling process ~~Thus, special attention should be paid to land–sea interactions~~ in future model development~~s~~.

Our comparison ~~of parameterization schemes~~a indicates ~~shows~~ that the parameterization schemes with the best performance ~~the results produced~~ for inland stations are generally consistent with those of previous investigations in this study,~~and that the same schemes show the best statistical scores~~ considering most of the stations are inland stations (89 out of 105 stations), this result is not surprising~~. Nonetheless, the ranking of scheme performance for~~, however, for coastal stations, the result is ~~was~~

different. For instance, ~~when comparing PBL schemes, the~~ MYNN ~~scheme~~ show~~ed~~ the ~~highest~~ best CORR score ~~value~~among the PBL schemes, while LES (YSU) shows the best BIAS (RMSE) score ~~had the smallest BIAS value and YSU had the smallest RMSE value~~. ~~However, for LW/SW radiation~~For SW-LW schemes, ~~the RRTMG and~~ Goddard shows the best scores of CORR, BIAS and RMSE, while Dudhia-RRTM ranks worst according to the CORR score. ~~schemes showed the highest CORR values, but had the smallest BIAS and RMSE values. Finally, the combined Dudhia and RRTM scheme, which performed best in previous comparisons, showed poor temporal relationships with observational data in this study.~~

3.2.2 ~~Comparison among stations with different topography~~Elevation

Figure 12 shows the comparison for stations with different elevation (e.g., < 50m, 51 stations in total; >50 & < 250m, 36 stations in total; < 250m, 19 stations in total).~~A comparison was also made between stations with different elevations (below 50 m, between 50 m and 250 m, and above 250 m) (Figure 10). Our results show~~ Observation shows that peak wind speed decreases ~~reduced in tandem~~ with ~~the station's~~ increasing elevation during the study period; for example, the peak observed ~~modeled~~ wind speed of~~at~~ high-elevation stations (>250 m) ~~was~~ is 1.5 m/s slower than that of~~for~~ low-elevation stations (<50 m). However, the peak simulated wind speed is ~~simulated peak values were~~ generally ~~the same~~similar for stations with different elevation, which ~~created~~bring ~~a large model bias above the~~ larger model error for the high-elevation stations. As shown by~~in~~ the statistic scores, ~~Table 10, calculated~~ for each PBL, MP and SW-LW schemes, CORR generally decreases with increasing elevation, while BIAS and RMSE scores increase with elevation, thus the evaluation metrics tend to degrade with increasing elevation under stable conditions over the study area.~~values for high-elevation stations were almost twice as large as those for low-elevation stations~~.

Further comparison indicates that ~~Interestingly, model~~ for different parameterization types, the scheme with best performance~~s were~~ is generally similar ~~for stations~~ with different elevation, e.g., for the PBL scheme, MYJ is always best at all elevation categories according to the CORR score, and YSU is always best according to the BIAS and RMSE scores.~~s, and the combination of schemes that provided an optimized performance was mostly consistent with previous analyses. For example, MYJ was the PBL scheme with the highest CORR value, and the YSU scheme recorded the smallest BIAS and RMSE values out of all stations. Thus, as the WRF model uses terrain-following coordinates, surface topography does not induce new uncertainties into the simulation, although land–sea interaction does, as shown in section 3.2.1.~~

4. Discussion

In order to evaluate atmospheric properties that are crucial for air quality under stable conditions and investigate what drives the differences in wind speed, we compare the simulated wind field from the simulation with the best Taylor skill score (i.e., using YSU, Dudhia-RRTM and WDM6) to the station observations, meanwhile, the same simulation but with QNSE PBL scheme (i.e., using QNSE, Dudhia-RRTM and WDM6) is used for comparison between the PBL schemes. In addition, the impact of different options in YSU scheme and land surface model are also discussed in this section.

4.1 Spatial distribution of wind field

Figure 13 shows the spatial distribution of observed and simulated wind field during the study period, we choose 14:00 in local time as an example. The simulation using YSU, Dudhia-RRTM and WDM6 schemes is referred to as YSU, and the simulation using QNSE, Dudhia-RRTM and WDM6 is referred to as QNSE. YSU generally reproduces the wind field in the study area, especially in terms of wind speed. For example, the observed wind speed is lower on 13 January 2019, with the values lower than 2 m/s in many stations, while on 15 January 2019, the observed wind speed is higher than 4 m/s in most of the stations. In the simulation with YSU, wind speed is about 2 m/s on 13 January 2019 and higher than 4 m/s on 15 January 2019 over the study area, which is close to the observation. On the contrary, simulation with QNSE fails to reproduce the distribution of wind speed, and shows strong overestimation, especially over the mountain areas of the study area (Figure 1a), for example, the peak wind speed in simulation with QNSE exceeds 20 m/s on 15 January 2019, which is more than five times greater than the observation, this overestimation is consistent with the large positive bias in previous investigation of Figure 3. For the wind-direction simulation, YSU shows degraded performance compared to wind speed, and generally fails to reproduce the wind-direction distribution for most of the stations, QNSE also fails to do so.

4.2 Vertical profile of wind speed

Figure 14 shows the observed and simulated vertical profile of wind speed at 08:00 and 20:00 during the study period, the location of the sounding station is illustrated in Figure 1. YSU reproduces the vertical structure of wind speed reasonably, with slightly larger model bias above the height of 15 km. Within the low levels below 2.5 km, simulated wind speed from the YSU scheme is close to the observation, with the bias lower than 2.5 m/s in most cases. Meanwhile, QNSE shows worse performance in reproducing the vertical structure of wind speed, with significant larger model bias compared to YSU. for example, QNSE overestimates the low-level (< 2.5 km) wind speed by about 10 m/s at 20:00 on 11 January 2019, and overestimate wind speed by 20 m/s at 20:00 on 11 January 2019. It is interesting to note that the simulation with QNSE is pretty similar to that with YSU at 08:00 during the study period, indicating that large difference between YSU and QNSE only occurs at specific time during the study period, which is also revealed in Figure 3a.

4.3 Impact of options in the YSU scheme

The impact of different options in YSU on wind-speed simulation is illustrated in Figure 15, the simulation with the best Taylor skill score in previous investigation is selected and referred to as YSU, three extra simulations with top-down mixing option turning off (No_mix), topographic correction option turning off (No_topo), and both options turning off (No_topo_mix) are conducted for comparison. The simulated wind speed increases when we turn off the individual or both options, which enlarges the overestimation of wind speed under stable condition in our study (Figure 15a). Further investigation indicates that turning off the two options in YSU mainly degrades model performance with worse evaluation metrics, for example, the BIAS score increases from 0.36 m/s to 0.67 m/s in No_topo, to 0.43 m/s in No_mix, and to 0.69 m/s in No_topo_mix, the RMSE scores shows similar degradation to BIAS by turning off the options in YSU.

4.4 Impact of land surface model

Figure 16 shows the evaluation of different land surface parameterizations with the same model configuration as the simulation with best the Taylor skill score, the land surface models (LSM) considered are the five-layer thermal diffusion scheme (SLAB, Dudhia, 1996), the Noah scheme (NOAH, Chen and Dudhia, 2001), the Rapid Update Cycle scheme (RUC, Smirnova et al., 2000), the Noah-MP scheme (NOAHMP), and the Community Land Model Version 4 scheme (CLM4, Lawrence et al., 2011). The simulations with different LSMs reproduce the timeseries of wind speed well, with larger spread among the LSMs during 14-15 January 2019 (Figure 16a). NOAHMP shows the best CORR score of 0.94, CLM4 and NOAH are slightly worse according to this score. Meanwhile, according to the RMSE score, NOAHMP is the best scheme, followed by RUC and NOAH. In addition, RUC and NOAHMP show better BIAS scores than the other LSMs. Thus, NOAHMP shows the best performance among different LSMs in wind-speed simulation under stable condition in this study, however, the large difference among LSMs indicates that we should take land surface parameterizations into consideration in future studies.

4.5 Impact of choice of ensemble

In this study, CORR, BIAS and RMSE are used as verification scores, CORR is a measure of the strength and direction of the linear relationship between simulation and observation, BIAS is a measure of mean difference between simulation and observation, and RMSE is the square root of the average of the set of squared differences between simulation and observation, thus each of this score gives a partial view of the model performance, and some schemes perform best according to one metric and worst according to another in our previous investigation.

As none of the schemes is the best according to all the scores, model ensemble is used to provide optimizing model performance, at the same time, model ensemble also provide probabilistic evaluation of the simulations as ensembles with narrow spread are often overconfident. The ensemble mean of 576 simulations in our study shows the best CORR score (0.94) in wind-speed simulation, however, this best CORR score is also result of single-model simulation with Goddard MP scheme. At the same time, the best wind-speed BIAS score (0.33 m/s) is result of the single-model simulation with MYDM7 or ETA, and the best RMSE score (0.52 m/s) is result of either the single-model simulation with Goddard, NSSL1, MYDM7, or the ensemble using the 3, 4 or 5 best simulations. Thus, model ensemble does not always provide the best performance, and model post-processing, especially the bias correction techniques are needed to taken into consideration, which can significantly reduce the systematic errors in model simulation. In addition, the PBL schemes play a dominant role in wind simulation, further tuning of the parameters within the PBL schemes, such as turbulent kinetic energy (TKE) dissipation rate, TKE diffusion factor, and turbulent length-scale coefficients is needed. Finally, it is worth pointing out that the presented findings in this study could be unique to the meteorological setup of the event, the location, the input dataset, the domain setup, and other unchanged parameterization types or model settings.

~~Finally, we note that the ensemble mean results reproduced the characteristics of the wind field more accurately than those of individual simulations, which indicates that constructing an ensemble was a more effective technique for optimizing model performance in this case. However, this does not imply that ensemble studies always provide a better and deeper understanding of related physical processes and interactions. Additional tuning of the parameters within key PBL schemes, such as YSU, are needed to achieve this goal, which is the focus of our future work.~~

5. Conclusion remarks~~s and discussion~~

In this study, we investigate wind simulations during a relatively long period of stable conditions when a haze event affected North China.~~d the impacts of physical parameterization schemes on simulated wind fields that generate under stable weather conditions~~. Surface meteorological observations are used to evaluate the WRF model's ability to predict the evolution of winds during the event. A number of WRF sensitivity experiments (640 in total) are conducted, altering the PBL, radiation, and microphysical schemes to determine the sensitivity of wind speed and direction simulations to choice of model physical ~~This was achieved by performing sensitivity simulations over the coastal regions of North China, which were characterized by a horizontal resolution of 0.5 km and considered PBL, MP, and LW/SW radiation physical components. A total of 640 simulations were conducted, which considered combinations of 10 different PBL schemes, 16 different MP schemes, and four different LW/SW schemes. The~~parameterizations. ~~influence of these parameterization schemes on simulated wind speeds and directions were analyzed using weather station observations as validation data.~~ Further investigations considering the ocean proximity and elevation~~underlying land type and topography~~ are~~were~~ conducted to provide ~~more complete~~deeper insight into the factors that influence model sensitivities.

In general, the WRF model reproduce~~sd~~ the temporal variation of wind speed ~~and direction~~ over the study area ~~to a high degree of accuracy~~well,~~.~~ the spread in wind speed are largest within the PBL schemes tested, followed by radiation, and then microphysics schemes.~~The simulated wind speed is most sensitive to the PBL scheme chosen, and to a lesser degree to the LW/SW radiation and MP schemes. Simulated~~ The wind direction is notably worse reproduced by WRF compared to wind speed~~ less sensitive to the choice of parameterization~~. This result is consistent with the findings of previous simulations performed in other locations (Dzebre and Adaramola, 2020; Gómez-Navarro et al., 2015; Santos-Alamillos et al., 2013).

Among all PBL schemes, MYJ shows the best CORR score of 0.96, MYNN, ACM2 and UW are slightly worse according to this score. YSU is the best scheme according to the BIAS and RMSE scores (0.45 m/s and 0.61 m/s), flowed by MYNN (0.55 m/s and 0.70 m/s). For the SW-LW and MP schemes, the CORR scores are similar, and Dudhia−RRTM and MYDM7 show the best model performances out of all SW-LW and MP schemes according to the BIAS and RMSE scores.~~The MYJ scheme showed the closest correlation with observation data among all of the considered PBL schemes, while the YSU scheme exhibited the smallest values for BIAS and RMSE. However, the QNSE scheme, which produced unrealistic model errors during daytime periods, is not suitable for the study area. The combined Dudhia and RRTM schemes, and the individual MYDM7 scheme both show the best model performances when compared with other LW/SW radiation and MP schemes, as defined by their high CORR values, low BIAS values, and low RMSE values.~~The Interactions among physical parameterization schemes~~components~~ also play an important role in wind simulations, as the best verification scores can only be achieved by certain combination of schemes~~, and can either increase or decrease the accuracy of the simulation. Choosing the appropriate number of members in an ensemble is vital for precise wind simulation; here, an ensemble mean comprised of the best four individual configurations substantially reduced overestimation of wind speed and provided the best combined~~

~~performance of all simulations.~~The ensemble mean of all the simulations shows the highest CORR core in wind speed, while the best 10 simulations show much better performance than the ensemble in terms of BIAS and RMSE.

~~The conclusions stated above are directly applicable for inland weather stations;~~ The schemes with the best performance for the inland stations are consistent to previous results, as the majority of stations are inland stations, however, for coastal stations, ~~the MYNN scheme showed the highest CORR value of~~ MYNN is the best scheme among all PBL schemes according to CORR, while LES (YSU) shows the best BIAS (RMSE) score ~~while the LES and YSU schemes showed the smallest BIAS and RMSE values, respectively. The RRTMG and Goddard schemes showed the highest CORR and smallest BIAS and RMSE values of all LW/SW radiation schemes~~. For SW-LW schemes, Goddard shows the best scores of CORR, BIAS and RMSE, while Dudhia-RRTM ranks worst according to the CORR score. ~~Our modeling also showed that performances are generally the same for stations located at different elevations.~~ The schemes with the best performance are similar with different elevation for different parameterization types, however, model performance tends to degrade with increasing elevation.

A large number of WRF simulations altering the PBL, MP, and radiation schemes are conducted in this study to investigate the model sensitivity of wind speed and direction to parameterizations under stable conditions over North China, the horizontal resolution of 0.5 km belongs to the PBL gray zone, which has rarely been used in previous simulation studies in China, the results of this study provide a valuable reference for other simulations over North China.

~~We conducted an innovative and thorough evaluation of model performance for wind simulation during a typical severe pollution event over North China. Further, to test the sensitivity of the model, we considered all possible combinations of physical parameterization schemes that are available. This model also used a horizontal resolution belonging to the PBL "gray zone", which has rarely been used in previous simulation studies. The findings of this study therefore provide a foundation for future research in this region, as well as a benchmark for investigation of other localities worldwide.~~

~~Finally, we note that the ensemble mean results reproduced the characteristics of the wind field more accurately than those of individual simulations, which indicates that constructing an ensemble was a more effective technique for optimizing model performance in this case. However, this does not imply that ensemble studies always provide a better and deeper understanding of related physical processes and interactions. Additional tuning of the parameters within key PBL schemes, such as YSU, are needed to achieve this goal, which is the focus of our future work.~~

Code and data availability

The Weather Research and Forecasting (WRF) model is freely available online and can be downloaded from the page: https://github.com/wrf-model/WRF. The ERA5 data are available at ECMWF (https://www.ecmwf.int/en/forecasts/datasets/reanalysis-datasets/era5). The CLARA product are available at Climate Data Store (https://cds.climate.copernicus.eu/cdsapp#!/dataset/satellite-cloud-properties?tab=overview). The observations and model's hourly output upon which this work is based are available at Zonodo (https://doi.org/10.5281/zenodo.6505423), all the results can also be obtained from yuet@mail.iap.ac.cn.

Author contributions

EY conceptualized the study and conducted the simulations. The analysis was carried out by all the authors. The original draft of the paper was written by EY, all the authors took part in the edition and revision of it.

Competing interests

The authors declare that they have no conflict of interest.

Acknowledgements

This work was supported by the National Natural Science Foundation of China (No. 42088101 and 42075168), the Technology Innovation Guidance Program of Hebei Province (No. 21475401D) and the National Key Research and Development Program of China (No. 2020YFF0304401). The simulation was supported by the National Key Scientific and Technological Infrastructure project "Earth System Numerical Simulation Facility" (EarthLab).

References

Angevine, W. M., Jiang, H., and Mauritsen, T.: Performance of an eddy diffusivity–mass flux scheme for shallow cumulus boundary layers, Mon Weather Rev, 138, 2895-2912, 2010.

Barlage, M., Miao, S., Chen, F.: Impact of physics parameterizations on high-resolution weather prediction over two Chinese megacities, Journal of Geophysical Research: Atmospheres 121, 4487-4498, 2016.

Bougeault, P. and Lacarrere, P.: Parameterization of orography-induced turbulence in a mesobeta--scale model, Mon Weather Rev, 117, 1872-1890, 1989.

Bretherton, C. S. and Park, S.: A new moist turbulence parameterization in the Community Atmosphere Model, Journal of Climate, 22, 3422-3448, 2009.

Cai, W., Li, K., Liao, H., Wang, H., and Wu, L.: Weather conditions conducive to Beijing severe haze more frequent under climate change, Nat. Clim. Chang., 7, 257-262, 10.1038/nclimate3249, 2017.

Carvalho, D., Rocha, A., Gómez-Gesteira, M., and Silva Santos, C.: Offshore wind energy resource simulation forced by different reanalyses: Comparison with observed data in the Iberian Peninsula, Applied Energy, 134, 57-64, https://doi.org/10.1016/j.apenergy.2014.08.018, 2014a.

Carvalho, D., Rocha, A., Gómez-Gesteira, M., and Silva Santos, C.: Sensitivity of the WRF model wind simulation and wind energy production estimates to planetary boundary layer parameterizations for onshore and offshore areas in the Iberian Peninsula, Applied Energy, 135, 234-246, https://doi.org/10.1016/j.apenergy.2014.08.082, 2014b.

Chang, R., Zhu, R., Badger, M., Hasager, C. B., Xing, X., and Jiang, Y.: Offshore Wind Resources Assessment from Multiple Satellite Data and WRF Modeling over South China Sea, Remote Sens-Basel, 7, 467-487, 2015.

Chen, F., and Dudhia, J.: Coupling an advanced land-surface hydrology model with the Penn State-NCAR MM5 modeling system. Part I: Model description and implementation, Mon. Weather Rev., 129, 569–585, 2001.

Chen, S. H. and Sun, W. Y.: A one-dimensional time dependent cloud model, Journal of the Meteorological Society of Japan. Ser. II, 80, 99-118, 2002.

Cheng, W. Y. Y., Liu, Y., Liu, Y., Zhang, Y., Mahoney, W. P., and Warner, T. T.: The impact of model physics on numerical wind forecasts, Renewable Energy, 55, 347-356, https://doi.org/10.1016/j.renene.2012.12.041, 2013.

Collins, W. D., Rasch, P. J., Boville, B. A., Hack, J. J., McCaa, J. R., Williamson, D. L., Kiehl, J. T., Briegleb, B., Bitz, C., and Lin, S.-J.: Description of the NCAR community atmosphere model (CAM 3.0), NCAR Tech. Note NCAR/TN-464+ STR, 226, 1326-1334, 2004.

Deardorff, J.: Sub-grid-scale turbulence modeling. Advances in Geophysics, Academic Press, 28, 337–343, https://doi.org/10.1016/S0065-2687(08)60193-4, 1985.

Dudhia, J.: Numerical study of convection observed during the winter monsoon experiment using a mesoscale two-dimensional model, Journal of Atmospheric Sciences, 46, 3077-3107, 1989.

Dudhia, J.: A multi-layer soil temperature model for MM5, in 6th PSU/NCAR Mesoscale Model Users' Workshop, Boulder, Colo, 49–50, 1996.

Dzebre, D. E. K. and Adaramola, M. S.: A preliminary sensitivity study of Planetary Boundary Layer parameterisation schemes in the weather research and forecasting model to surface winds in coastal Ghana, Renewable Energy, 146, 66-86, https://doi.org/10.1016/j.renene.2019.06.133, 2020.

Eaton, B.: User's guide to the Community Atmosphere Model CAM-5.1, NCAR. URL http://www.cesm. ucar. edu/models/cesm1. 0/cam, 2011.

Falasca, S., Gandolfi, I., Argentini, S., Barnaba, F., Casasanta, G., Di Liberto, L., Petenko, I., and Curci, G.: Sensitivity of near-surface meteorology to PBL schemes in WRF simulations in a port-industrial area with complex terrain, Atmospheric Research, 264, 105824, https://doi.org/10.1016/j.atmosres.2021.105824, 2021.

Fernández-González, S., Martín, M. L., García-Ortega, E., Merino, A., Lorenzana, J., Sánchez, J. L., Valero, F., Rodrigo, J. S.: Sensitivity Analysis of the WRF Model: Wind-Resource Assessment for Complex Terrain, Journal of Applied Meteorology and Climatology, 57(3), 733-753, 2018.

Gan, Y., Liang, X.-Z., Duan, Q., Chen, F., Li, J., and Zhang, Y.: Assessment and Reduction of the Physical Parameterization Uncertainty for Noah-MP Land Surface Model, Water Resources Research, 55, 5518-5538, https://doi.org/10.1029/2019WR024814, 2019.

Gao, M., Carmichael, G. R., Wang, Y., Saide, P. E., Yu, M., Xin, J., Liu, Z., and Wang, Z.: Modeling study of the 2010 regional haze event in the North China Plain, Atmos. Chem. Phys., 16, 1673–1691, 2016a.

Gao, X., Shi, Y., and Giorgi, F.: Comparison of convective parameterizations in RegCM4 experiments over China with CLM as the land surface model, Atmospheric and Oceanic Science Letters, 9, 246-254, 10.1080/16742834.2016.1172938, 2016b.

Gholami, S., Ghader, S., Khaleghi-Zavareh, H., and Ghafarian, P.: Sensitivity of WRF-simulated 10 m wind over the Persian Gulf to different boundary conditions and PBL parameterization schemes, Atmospheric Research, 247, 105147, https://doi.org/10.1016/j.atmosres.2020.105147, 2021.

Gómez-Navarro, J. J., Raible, C. C., and Dierer, S.: Sensitivity of the WRF model to PBL parametrisations and nesting techniques: evaluation of wind storms over complex terrain, Geosci. Model Dev., 8, 3349-3363, 10.5194/gmd-8-3349-2015, 2015.

Gonçalves-Ageitos, M., Barrera-Escoda, A., Baldasano, J. M., and Cunillera, J.: Modelling wind resources in climate change scenarios in complex terrains, Renewable energy, 76, 670-678, 2015.

Hersbach, H., Bell, B., Berrisford, P., Hirahara, S., Horányi, A., Muñoz-Sabater, J., Nicolas, J., Peubey, C., Radu, R., Schepers, D. and Simmons, A.: The ERA5 global reanalysis. Quarterly Journal of the Royal Meteorological Society, 146, 1999-2049, 2020.

Hong, S.-Y. and Lim, J.-O. J.: The WRF single-moment 6-class microphysics scheme (WSM6), Asia-Pacific Journal of Atmospheric Sciences, 42, 129-151, 2006.

Hong, S.-Y., Dudhia, J., and Chen, S.-H.: A revised approach to ice microphysical processes for the bulk parameterization of clouds and precipitation, Mon Weather Rev, 132, 103-120, 2004.

Hong, S., Noh, Y., and Dudhia, J.: A new vertical diffusion package with an explicit treatment of entrainment processes, Mon Weather Rev, 134, 2318-2341, 2006.

Honnert, R., Couvreux, F., Masson, V., Lancz, D.: Sampling the structure of convective turbulence and implications for grey-zone parametrizations, Boundary-Layer Meteorol, 160, 133–156, 2016.

Hua, W., Wu, B.: Atmospheric circulation anomaly over mid- and high-latitudes and its association with severe persistent haze events in Beijing, Atmospheric Research, 277, 106315, 2022.

Iacono, M. J., Delamere, J. S., Mlawer, E. J., Shephard, M. W., Clough, S. A., and Collins, W. D.: Radiative forcing by long-lived greenhouse gases: Calculations with the AER radiative transfer models, Journal of Geophysical Research: Atmospheres, 113, 2008.

Janjić, Z. I.: The step-mountain eta coordinate model: Further developments of the convection, viscous sublayer, and turbulence closure schemes, Mon Weather Rev, 122, 927-945, 1994.

Jiménez, P. A. and Dudhia, J.: Improving the representation of resolved and unresolved topographic effects on surface wind in the WRF model, J Appl Meteorol Clim, 51, 300-316, 2012.

Jimenez, P. A., Dudhia, J., Fidel Gonzalez–Rouco, J., Navarro, J., Montavez J., and Garcia-Bustamante, E.: A revised scheme for the WRF surface layer formulation. Mon. Wea. Rev., 140, 898–918, 2012.

Karlsson, K., Riihelä, A., Trentmann, J., Stengel, M., Meirink, J., Solodovnik, I., Devasthale, A., Manninen, T., Jääskeläinen, E., Anttila, K., Kallio-Myers, V., Benas, N., Selbach, N., Stein, D., Kaiser, J., Hollmann, R.: ICDR AVHRR-based on CLARA-

A2 methods, Satellite Application Facility on Climate Monitoring, doi:10.5676/EUM_SAF_CM/CLARA_AVHRR/V002_01, 2021.

Kong, X., Wang, A., Bi, X., Sun, B., and Wei, J.: The hourly precipitation frequencies in the tropical-belt version of WRF: sensitivity to cumulus parameterization and radiative schemes, Journal of Climate, 1-59, 10.1175/jcli-d-20-0854.1, 2021.

Lawrence, D., Oleson, K., Flanner, M., Thornton, P., Swenson, S., Lawrence, P., Zeng, X., Yang, Z., Levis, S., Sakaguchi, K., Bonan, G., Slater, A.: Parameterization improvements and functional and structural advances in Version 4 of the Community Land Model, J. Adv. Model. Earth Syst., 3, M03001, doi:10.1029/2011MS00045, 2011.

Li, J., Ding, C., Li, F., and Chen, Y.: Effects of single- and double-moment microphysics schemes on the intensity of super typhoon Sarika (2016), Atmospheric Research, 238, 104894, https://doi.org/10.1016/j.atmosres.2020.104894, 2020.

Li, M., Tang, G., Huang, J., Liu, Z., An, J., and Wang, Y.: Characteristics of winter atmospheric mixing layer height in Beijing-Tianjin-Hebei region and their relationship with the atmospheric pollution (in Chinese), Enviromental Science, 36, 1935-1943, 10.13227/j.hjkx.2015.06.004, 2015.

Li, S., Sun, X., Zhang, S., Zhao, S., and Zhang, R.: A Study on Microscale Wind Simulations with a Coupled WRF–CFD Model in the Chongli Mountain Region of Hebei Province, China, Atmosphere-Basel, 10, 731, 2019.

Lim, K.-S. S. and Hong, S.-Y.: Development of an effective double-moment cloud microphysics scheme with prognostic cloud condensation nuclei (CCN) for weather and climate models, Mon Weather Rev, 138, 1587-1612, 2010.

Lin, Y. and Colle, B. A.: A new bulk microphysical scheme that includes riming intensity and temperature-dependent ice characteristics, Mon Weather Rev, 139, 1013-1035, 2011.

Mansell, E. R., Ziegler, C. L., and Bruning, E. C.: Simulated electrification of a small thunderstorm with two-moment bulk microphysics, Journal of Atmospheric Sciences, 67, 171-194, 2010.

Matsui, T., Zhang, S. Q., Lang, S. E., Tao, W.-K., Ichoku, C., and Peters-Lidard, C. D.: Impact of radiation frequency, precipitation radiative forcing, and radiation column aggregation on convection-permitting West African monsoon simulations, Clim Dyn, 55, 193-213, 2020.

Mesinger, F.: Forecasting upper tropospheric turbulence within the framework of the Mellor-Yamada 2.5 closure, Res. Activ. Atmos. Oceanic Mod., 1993.

Milbrandt, J. and Yau, M.: A multimoment bulk microphysics parameterization. Part I: Analysis of the role of the spectral shape parameter, Journal of the atmospheric sciences, 62, 3051-3064, 2005.

Mirocha, J., Lundquist, J., and Kosović, B.: Implementation of a nonlinear subfilter turbulence stress model for large-eddy simulation in the Advanced Research WRF model, Mon Weather Rev, 138, 4212-4228, 2010.

Mlawer, E. J., Taubman, S. J., Brown, P. D., Iacono, M. J., and Clough, S. A.: Radiative transfer for inhomogeneous atmospheres: RRTM, a validated correlated-k model for the longwave, Journal of Geophysical Research: Atmospheres, 102, 16663-16682, 1997.

Morrison, H. and Milbrandt, J. A.: Parameterization of cloud microphysics based on the prediction of bulk ice particle properties. Part I: Scheme description and idealized tests, Journal of Atmospheric Sciences, 72, 287-311, 2015.

Morrison, H., Thompson, G., and Tatarskii, V.: Impact of cloud microphysics on the development of trailing stratiform precipitation in a simulated squall line: Comparison of one-and two-moment schemes, Mon Weather Rev, 137, 991-1007, 2009.

Nakanishi, M. and Niino, H.: Development of an improved turbulence closure model for the atmospheric boundary layer, Journal of the Meteorological Society of Japan. Ser. II, 87, 895-912, 2009.

Niu, G. Y., Yang, Z. L., Mitchell, K. E., Chen, F., Ek, M. B., Barlage, M., Kumar, A., Manning, K., Niyogi, D., and Rosero, E.: The community Noah land surface model with multiparameterization options (Noah-MP): 1. Model description and evaluation with local-scale measurements, Journal of Geophysical Research: Atmospheres, 116, 2011.

Pan, L., Liu, Y., Roux, G., Cheng, W., Liu, Y., Hu, J., Jin, S., Feng, S., Du, J., and Peng, L.: Seasonal variation of the surface wind forecast performance of the high-resolution WRF-RTFDDA system over China, Atmospheric Research, 259, 105673, https://doi.org/10.1016/j.atmosres.2021.105673, 2021.

Pleim, J. E.: A combined local and nonlocal closure model for the atmospheric boundary layer. Part I: Model description and testing, J Appl Meteorol Clim, 46, 1383-1395, 2007.

Prieto-Herráez, D., Frías-Paredes, L., Cascón, J. M., Lagüela-López, S., Gastón-Romeo, M., Asensio-Sevilla, M. I., Martín-Nieto, I., Fernandes-Correia, P. M., Laiz-Alonso, P., Carrasco-Díaz, O. F., Sáez-Blázquez, C., Hernández, E., Ferragut-Canals, L., and González-Aguilera, D.: Local wind speed forecasting based on WRF-HDWind coupling, Atmospheric Research, 248, 105219, https://doi.org/10.1016/j.atmosres.2020.105219, 2021.

Puliafito, S. E., Allende, D. G., Mulena, C. G., Cremades, P., and Lakkis, S. G.: Evaluation of the WRF model configuration for Zonda wind events in a complex terrain, Atmospheric Research, 166, 24-32, https://doi.org/10.1016/j.atmosres.2015.06.011, 2015.

Rajeevan, M., Kesarkar, A., Thampi, S. B., Rao, T. N., Radhakrishna, B., and Rajasekhar, M.: Sensitivity of WRF cloud microphysics to simulations of a severe thunderstorm event over Southeast India, Ann. Geophys., 28, 603-619, 10.5194/angeo-28-603-2010, 2010.

Rogers, E., Black, T., Ferrier, B., Lin, Y., Parrish, D., and DiMego, G.: Changes to the NCEP Meso Eta Analysis and Forecast System: Increase in resolution, new cloud microphysics, modified precipitation assimilation, modified 3DVAR analysis, NWS Technical Procedures Bulletin, 488, 15, 2001.

Rybchuk, A., Optis, M., Lundquist, J. K., Rossol, M., and Musial, W.: A Twenty-Year Analysis of Winds in California for Offshore Wind Energy Production Using WRF v4.1.2, Geosci. Model Dev. Discuss., 2021, 1-41, 10.5194/gmd-2021-50, 2021.

Santos-Alamillos, F. J., Pozo-Vázquez, D., Ruiz-Arias, J. A., Lara-Fanego, V., and Tovar-Pescador, J.: Analysis of WRF Model Wind Estimate Sensitivity to Physics Parameterization Choice and Terrain Representation in Andalusia (Southern Spain), J Appl Meteorol Clim, 52, 1592-1609, 10.1175/jamc-d-12-0204.1, 2013.

Shin, H. H. and Hong, S.: Representation of the subgrid-scale turbulent transport in convective boundary layers at gray-zone resolutions, Mon Weather Rev, 143, 250-271, 2015.

Skamarock, W. C., Klemp, J. B., Dudhia, J., Gill, D. O., Barker, D. M., Wang, W., and Powers, J. G.: A description of the Advanced Research WRF version 3, NCAR Technical note-475+ STR, 2008.

Smirnova, T. G., Brown, J. M., Benjamin, S. G., and Kim D.: Parameterization of cold-season processes in the MAPS land surface scheme, J. Geophys. Res., 105, 4077–4086, doi:10.1029/1999JD901047, 2000.

Song, M., Wu, J., Song, M., Zhang, L., Zhu, Y.: Spatiotemporal regularity and spillover effects of carbon emission intensity in China's Bohai Economic Rim, Science of The Total Environment, 740, 140184, 2020.

Stegehuis, A. I., Vautard, R., Ciais, P., Teuling, A. J., Miralles, D. G., and Wild, M.: An observation-constrained multi-physics WRF ensemble for simulating European mega heat waves, Geosci. Model Dev., 8, 2285-2298, 10.5194/gmd-8-2285-2015, 2015.

Sukoriansky, S., Galperin, B., and Perov, V.: Application of a new spectral theory of stably stratified turbulence to the atmospheric boundary layer over sea ice, Boundary-layer meteorology, 117, 231-257, 2005.

Tao, W.-K., Simpson, J., and McCumber, M.: An ice-water saturation adjustment, Mon Weather Rev, 117, 231-235, 1989.

Taraphdar, S., Pauluis, O. M., Xue, L., Liu, C., Rasmussen, R., Ajayamohan, R. S., Tessendorf, S., Jing, X., Chen, S., and Grabowski, W. W.: WRF Gray-Zone Simulations of Precipitation Over the Middle-East and the UAE: Impacts of Physical Parameterizations and Resolution, Journal of Geophysical Research: Atmospheres, 126, e2021JD034648, https://doi.org/10.1029/2021JD034648, 2021.

Thompson, G. and Eidhammer, T.: A study of aerosol impacts on clouds and precipitation development in a large winter cyclone, Journal of the atmospheric sciences, 71, 3636-3658, 2014.

Thompson, G., Field, P. R., Rasmussen, R. M., and Hall, W. D.: Explicit forecasts of winter precipitation using an improved bulk microphysics scheme. Part II: Implementation of a new snow parameterization, Mon Weather Rev, 136, 5095-5115, 2008.

Tiedtke, M.: A comprehensive mass flux scheme for cumulus parameterization in large–scale models. Mon. Wea. Rev., 117, 1779–1800, 1989.

Ulpiani, G.: On the linkage between urban heat island and urban pollution island: Three-decade literature review towards a conceptual framework, Science of The Total Environment, 751, 141727, https://doi.org/10.1016/j.scitotenv.2020.141727, 2021.

Wang, H., Yu, E., and Yang, S.: An exceptionally heavy snowfall in Northeast china: large-scale circulation anomalies and hindcast of the NCAR WRF model, Meteorology and Atmospheric Physics, 113, 11-25, 10.1007/s00703-011-0147-7, 2011.

Wang, T., Zhang, M., and Han, X.: Source Apportionment of PM2.5 during a Heavy Pollution Episode in Qinhuangdao in Winter 2019 Using a Chemical Transport Model, Climatic and Environmental Research (in Chinese), 26, 471-481, 2021.

Wang, X. and Mauzerall, D. L.: Evaluating impacts of air pollution in China on public health: Implications for future air pollution and energy policies, Atmos Environ, 40, 1706-1721, https://doi.org/10.1016/j.atmosenv.2005.10.066, 2006.

Xia, G., Zhou, L., Minder, J. R., Fovell, R. G., and Jimenez, P. A.: Simulating impacts of real-world wind farms on land surface temperature using the WRF model: physical mechanisms, Clim Dyn, 53, 1723-1739, 10.1007/s00382-019-04725-0, 2019.

Yang, B., Qian, Y., Berg, L. K., Ma, P.-L., Wharton, S., Bulaevskaya, V., Yan, H., Hou, Z., and Shaw, W. J.: Sensitivity of Turbine-Height Wind Speeds to Parameters in Planetary Boundary-Layer and Surface-Layer Schemes in the Weather Research and Forecasting Model, Boundary-Layer Meteorology, 162, 117-142, 10.1007/s10546-016-0185-2, 2017.

Yang, Z., Niu, G., Mitchell, K. E., Chen, F., Ek, M. B., Barlage, M., Longuevergne, L., Manning, K., Niyogi, D., and Tewari, M.: The community Noah land surface model with multiparameterization options (Noah-MP): 2. Evaluation over global river basins, Journal of Geophysical Research: Atmospheres, 116, 2011.

Yu, E., Wang, H., Gao, Y., and Sun, J.: Impacts of cumulus convective parameterization schemes on summer monsoon precipitation simulation over China, Acta Meteorologica Sinica, 25, 581-592, 2011.

Yu, E., Wang, H., Sun, J., Gao, Y.: Climatic response to changes in vegetation in the Northwest Hetao Plain as simulated by the WRF model, International Journal of Climatology, 33, 1470-1481, 2013.

Zhang, L., Wang, T., Lv, M., and Zhang, Q.: On the severe haze in Beijing during January 2013: Unraveling the effects of meteorological anomalies with WRF-Chem, Atmos Environ, 104, 11-21, https://doi.org/10.1016/j.atmosenv.2015.01.001, 2015.

Zhang, R., Li, Q., and Zhang, R.: Meteorological conditions for the persistent severe fog and haze event over eastern China in January 2013, Science China Earth Sciences, 57, 26-35, 10.1007/s11430-013-4774-3, 2014.

Zhao, J., Guo, Z., S, Z., Zhao, Z., Xiao, X., Liu, F.: An improved multi-step forecasting model based on WRF ensembles and creative fuzzy systems for wind speed, Applied Energy, 162, 808-826, 2016.

Zhao, Y., Zhou, J., Fan, Y., Feng, M., Zhang, Z.: Economic and environmental impacts of China's imported iron ore transport chain under road-to-rail policy: an empirical analysis based on the Bohai Economic Rim, Carbon Management, 11:6, 653-671, 2020.

Zhou, X., Yang, K., Beljaars, A., Li, H., Lin, C., Huang, B., and Wang, Y.: Dynamical impact of parameterized turbulent orographic form drag on the simulation of winter precipitation over the western Tibetan Plateau, Clim Dyn, 53, 707-720, 10.1007/s00382-019-04628-0, 2019.

Table 1: List of microphysics (MP), planetary boundary layer (PBL), shortwave-longwave radiation (SW-LW) schemes investigated in this study.

MP	PBL	SW	LW
Purdue Lin (Lin; Chen and Sun, 2002)	LES(Mirocha et al., 2010)	Dudhia(Dudhia, 1989)	RRTM(Mlawer et al., 1997)
WRF single-moment 3-class (WSM3; Hong et al., 2004)	Yonsei University (YSU; Hong et al., 2006)	CAM(Collins et al., 2004)	CAM(Collins et al., 2004)
WRF single-moment 5-class (WSM5; Hong et al., 2004)	Mellor–Yamada–Janjic (MYJ; Janjić, 1994; Mesinger, 1993)	RRTMG(Iacono et al., 2008)	RRTMG(Iacono et al., 2008)
ETA Ferrier(ETA, Rogers et al., 2001)	Quasi-normal scale elimination (QNSE; Sukoriansky et al., 2005)	Goddard(Matsui et al., 2020)	Goddard(Matsui et al., 2020)
WRF single-moment 6-class (WSM6; Hong and Lim, 2006)	Mellor–Yamada Nakanishi Niino 2.5 level TKE (MYNN; Nakanishi and Niino, 2009)		
Goddard(Tao et al., 1989)	Asymmetric convection model 2 (ACM2; Pleim, 2007)		
Thompson(Thompson et al., 2008)	Bougeault–Lacarrere (BouLac; Bougeault and Lacarrere, 1989)		
Milbrandt-Yau double-moment 7-class (MYDM7; Milbrandt and Yau, 2005)	University of Washington (UW; Bretherton and Park, 2009)		
Morrison double moment (Morrison; Morrison et al., 2009)	TEMF(Angevine et al., 2010)		
CAM double-moment 5-class (CAM; Eaton, 2011)	Shin-Hong scale-aware(Shin-Hong, Shin and Hong, 2015)		
Stony-Brook University (SBU; Lin and Colle, 2011)			
WRF double-moment 6-class (WDM6; Lim and Hong, 2010)			
NSSL double moment (NSSL2; Mansell et al., 2010)			
NSSL single-moment 7-class (NSSL1, Mansell et al., 2010)			

Aerosol-Aware Thompson (ThompsonAA; Thompson and Eidhammer, 2014)			
P3(Morrison and Milbrandt, 2015)			

Table 2: List of default parameterization schemes for the simulation of outer domains (D01 and D02)

parameterization	D01 (8 km)	D02 (2 km)
Microphysics	SBU	SBU
Planetary boundary layer	Shin-Hong	Shin-Hong
Shortwave radiation	CAM	CAM
Longwave radiation	CAM	CAM
Culumus	Modifed Tiedtke (Tiedtke, 1989)	None
Land surface	Noah-MP (Niu et al., 2011; Yang et al., 2011)	Noah-MP

~~**Table 1: PBL scheme options investigated in this study.**~~

~~No~~	~~Scheme~~	~~Reference~~
~~1~~	~~LES~~	~~(Mirocha et al., 2010)~~
~~2~~	~~Yonsei University (YSU)~~	~~(Hong et al., 2006)~~
~~3~~	~~Mellor–Yamada–Janjic (MYJ)~~	~~(Janjić, 1994; Mesinger, 1993)~~
~~4~~	~~Quasi-normal scale elimination (QNSE)~~	~~(Sukoriansky et al., 2005)~~
~~5~~	~~Mellor–Yamada Nakanishi Niino (MYNN)~~	~~(Nakanishi and Niino, 2009)~~
~~6~~	~~Asymmetric convection model 2 (ACM2)~~	~~(Pleim, 2007)~~
~~7~~	~~Bougeault–Lacarrere (BouLac)~~	~~(Bougeault and Lacarrere, 1989)~~
~~8~~	~~University of Washington (UW)~~	~~(Bretherton and Park, 2009)~~
~~9~~	~~TEMF~~	~~(Angevine et al., 2010)~~
~~10~~	~~Shin–Hong scale-aware~~	~~(Shin and Hong, 2015)~~

Table 2: MP scheme options investigated in this study.

	Scheme	Reference
1	Purdue Lin (Lin)	(Chen and Sun, 2002)
2	WRF single-moment 3-class (WSM3)	(Hong et al., 2004)
3	WRF single-moment 5-class (WSM5)	(Hong et al., 2004)
4	ETA Ferrier	(Rogers et al., 2001)
5	WRF single-moment 6-class (WSM6)	(Hong and Lim, 2006)
6	Goddard	(Tao et al., 1989)
7	Thompson	(Thompson et al., 2008)
8	Milbrandt-Yau double-moment 7-class (MYDM7)	(Milbrandt and Yau, 2005)
9	Morrison double-moment (Morrison)	(Morrison et al., 2009)
10	CAM double-moment 5-class (CAM)	(Eaton, 2011)
11	Stony-Brook University (SBU)	(Lin and Colle, 2011)
12	WRF double-moment 6-class (WDM6)	(Lim and Hong, 2010)
13	NSSL double-moment (NSSL2)	(Mansell et al., 2010)
14	NSSL single-moment 7-class (NSSL1)	
15	Aerosol-Aware Thompson (ThompsonAA)	(Thompson and Eidhammer, 2014)
16	P3	(Morrison and Milbrandt, 2015)

830

Table 3: Radiation scheme options investigated in this study.

	Short-wave radiation		Long-wave radiation	
	Scheme	Reference	Scheme	Reference
1	Dudhia	(Dudhia, 1989)	RRTM	(Mlawer et al., 1997)
2	CAM	(Collins et al., 2004)	CAM	(Collins et al., 2004)
3	RRTMG	(Iacono et al., 2008)	RRTMG	(Iacono et al., 2008)
4	Goddard	(Matsui et al., 2020)	Goddard	(Matsui et al., 2020)

Table 4: Wind speed statistics averaged over the weather stations used different PBL schemes.

	CORR	BIAS	RMSE
LES	0.916	0.573	1.789
YSU	0.930	**0.448**	**1.585**
MYJ	**0.956**	0.928	2.010
QNSE	*0.643*	*3.218*	*4.839*
MYNN	0.941	0.553	1.732
ACM2	0.939	0.691	1.872
BouLac	0.917	0.831	2.036
UW	0.938	0.649	1.746
TEMF	0.894	1.015	1.884
Shin-Hong	0.930	0.705	1.738

Table 5: Wind direction statistics for different PBL schemes.

	CORR	BIAS	RMSE
LES	0.420	5.171	**36.646**
YSU	0.339	10.436	42.438
MYJ	0.280	8.218	38.406
QNSE	0.480	**1.670**	39.792
MYNN	0.234	8.110	40.013
ACM2	0.381	9.703	41.830
BouLac	**0.488**	13.153	43.495
UW	0.378	10.830	41.110
TEMF	0.317	7.267	39.900
Shin-Hong	0.284	11.661	42.365

Table 6: Statistics for wind speed and direction for different MP schemes.

	Wind speed			Wind direction		
	CORR	BIAS	RMSE	CORR	BIAS	RMSE
Lin	0.941	0.692	1.800	0.374	8.926	32.329
WSM3	0.939	0.771	1.824	0.340	10.829	34.007
WSM5	0.940	0.702	1.804	0.373	9.316	32.489
ETA	0.943	0.677	1.791	0.377	8.615	32.129
WSM6	0.940	0.703	1.805	0.366	9.295	32.616
Goddard	0.943	0.685	1.800	**0.395**	8.905	31.762
Thompson	0.942	0.695	1.792	0.372	8.653	32.239
MYDM7	**0.944**	**0.660**	**1.788**	0.392	**8.050**	**31.505**
Morrison	0.940	0.707	1.800	0.357	9.234	32.904
CAM5	0.940	0.742	1.805	0.344	10.366	33.756
SBU	0.938	0.762	1.821	0.343	10.820	34.066
WDM6	0.940	0.736	1.801	0.363	9.716	33.104
NSSL2	0.940	0.736	1.801	0.363	9.716	33.104
NSSL1	0.943	0.682	1.794	0.377	8.491	32.119
ThompsonAA	0.940	0.736	1.806	0.351	10.290	33.612
P3	0.942	0.670	1.789	0.380	8.151	31.737

Table 7: Statistics for wind speed and direction for different LW/SW radiation schemes.

	Wind speed			Wind direction		
	CORR	BIAS	RMSE	CORR	BIAS	RMSE
Dudhia and RRTM	**0.943**	**0.646**	**1.754**	0.355	9.155	32.765
CAM	0.941	0.736	1.834	**0.377**	9.276	**32.519**
RRTMG	0.939	0.763	1.842	0.370	9.983	33.054
Goddard	0.940	0.697	1.783	0.362	**9.040**	32.598

845

Table 8: Wind speed statistics for the top 10 schemes. The ensembles show the mean values for different numbers of the best simulations, shown in parentheses, alongside the mean values of all simulations (without QNSE).

	CORR	BIAS	RMSE
WDM6	0.934	0.361	0.530
Goddard	0.937	0.364	0.527
MYDM7	0.928	0.331	0.525
NSSL1	0.934	0.355	0.524
WSM5	0.930	0.370	0.545
Lin	0.931	0.370	0.544
P3	0.927	0.351	0.539
SBU	0.930	0.453	0.605
ETA	0.931	0.338	0.526
WSM6	0.931	0.370	0.544
Ensemble (2)	*0.936*	*0.362*	*0.528*
Ensemble (3)	*0.934*	*0.352*	*0.525*
Ensemble (4)	***0.934***	***0.352***	***0.524***
Ensemble (5)	*0.934*	*0.355*	*0.528*
Ensemble (7)	*0.933*	*0.357*	*0.531*
Ensemble (10)	*0.933*	*0.366*	*0.537*
Ensemble (all)	***0.937***	***0.686***	***0.808***

Notes: The PBL and LW/SW radiation schemes used in the 10 best schemes were YSU and Dudhia and RRTM.

Table 9: Wind speed statistics for coastal and inland stations.

		Costal stations			Inland stations		
		CORR	BIAS	RMSE	CORR	BIAS	RMSE
PBL	LES	0.790	**0.352**	0.844	0.912	0.607	0.818
	YSU	0.841	0.426	**0.732**	0.918	**0.456**	**0.638**
	MYJ	0.838	0.846	1.059	**0.951**	0.950	1.092
	MYNN	**0.856**	0.553	0.799	0.932	0.554	0.725
	ACM2	0.848	0.629	0.913	0.931	0.701	0.882
	BouLac	0.834	0.533	0.880	0.912	0.882	1.130
	UW	0.835	0.629	0.893	0.933	0.651	0.788
	TEMF	0.846	0.925	1.098	0.876	1.031	1.181
	Shin-Hong	0.850	0.687	0.902	0.919	0.709	0.849
MP	Lin	0.841	0.573	0.849	0.934	0.718	0.857
	WSM3	**0.871**	0.784	0.955	0.931	0.774	0.910
	WSM5	0.839	0.602	0.870	0.933	0.725	0.865
	ETA	0.850	0.537	0.815	0.935	0.707	0.845
	WSM6	0.839	0.602	0.870	0.933	0.726	0.865
	Goddrd	0.843	0.548	0.835	**0.936**	0.715	0.853
	Thompson	0.852	0.580	0.835	0.934	0.719	0.855
	MYDM7	0.846	**0.514**	**0.805**	**0.936**	**0.691**	**0.830**
	Morrison	0.848	0.615	0.864	0.932	0.728	0.866
	CAM5	0.864	0.745	0.932	0.931	0.746	0.882
	SBU	0.866	0.750	0.937	0.929	0.768	0.906
	WDM6	0.861	0.701	0.903	0.932	0.746	0.880
	NSSL2	0.861	0.701	0.903	0.932	0.746	0.880
	NSSL1	0.848	0.548	0.825	0.935	0.711	0.848
	ThompsonAA	0.867	0.724	0.912	0.931	0.742	0.880
	P3	0.843	0.532	0.821	0.935	0.700	0.839
RAD	Dudhia and RRTM	0.844	0.609	0.855	**0.937**	**0.652**	**0.787**
	CAM	0.852	0.610	0.865	0.933	0.758	0.900
	RRTMG	**0.857**	0.712	0.924	0.931	0.772	0.915
	Goddard	0.853	**0.550**	**0.811**	0.931	0.724	0.859

Table 10: Wind speed statistics for stations located at different altitudes

		<50 m			>50 m and <250 m			>250 m		
		CORR	BIAS	RMSE	CORR	BIAS	RMSE	CORR	BIAS	RMSE
PBL	LES	0.878	0.307	0.693	0.902	0.708	0.906	0.902	1.034	1.335
	YSU	0.910	**0.248**	**0.559**	0.868	**0.516**	**0.758**	0.868	**0.862**	**1.078**
	MYJ	**0.923**	0.599	0.766	**0.939**	1.052	1.188	**0.939**	1.584	1.982
	MYNN	0.913	0.374	0.618	0.904	0.590	0.801	0.904	0.971	1.319
	ACM2	0.916	0.470	0.694	0.912	0.755	0.940	0.912	1.171	1.576
	BouLac	0.890	0.566	0.865	0.905	0.976	1.194	0.905	1.269	1.728
	UW	0.919	0.453	0.657	0.901	0.683	0.847	0.901	1.115	1.436
	TEMF	0.895	0.823	0.982	0.845	1.074	1.247	0.845	1.428	1.733
	Shin-Hong	0.910	0.501	0.707	0.885	0.758	0.926	0.885	1.159	1.453
MP	Lin	0.916	0.454	0.668	0.916	0.788	0.931	0.916	1.179	1.493
	WSM3	0.922	0.587	0.750	0.915	0.823	0.966	0.915	1.195	1.504
	WSM5	0.913	0.471	0.685	0.916	0.792	0.935	0.916	1.179	1.491
	ETA	0.920	0.432	0.643	0.915	0.779	0.922	0.915	1.174	1.484
	WSM6	0.914	0.472	0.684	0.915	0.794	0.937	0.915	1.177	1.489
	Goddrd	0.917	0.442	0.659	**0.918**	0.784	0.925	**0.918**	1.181	1.495
	Thompson	0.921	0.461	0.660	0.914	0.787	0.930	0.914	1.174	1.485
	MYD7	0.919	0.407	**0.630**	0.917	**0.766**	**0.909**	0.917	1.168	1.480
	Morrison	0.918	0.483	0.681	0.912	0.792	0.938	0.912	1.173	1.484
	CAM5	0.923	0.550	0.719	0.913	0.797	0.941	0.913	1.180	1.489
	SBU	0.922	0.574	0.740	0.911	0.815	0.962	0.911	1.190	1.502
	WDM6	0.923	0.530	0.705	0.913	0.803	0.945	0.913	1.187	1.488
	NSSL2	0.923	0.530	0.705	0.913	0.803	0.945	0.913	1.187	1.488
	NSSL1	0.920	0.442	0.651	0.915	0.782	0.927	0.915	1.168	1.479
	ThompsonAA	**0.925**	0.535	0.705	0.911	0.799	0.946	0.911	1.179	1.488
	P3	0.916	**0.428**	0.650	0.917	0.771	0.913	0.917	**1.163**	**1.476**
RAD	Dudhia and RRTM	0.917	**0.436**	**0.648**	**0.921**	**0.707**	**0.847**	**0.921**	**1.099**	**1.416**
	CAM	0.919	0.497	0.692	0.915	0.827	0.973	0.915	1.210	1.526
	RRTMG	**0.921**	0.551	0.729	0.911	0.831	0.983	0.911	1.206	1.521
	Goddard	0.919	0.445	0.654	0.911	0.796	0.937	0.911	1.193	1.492

855

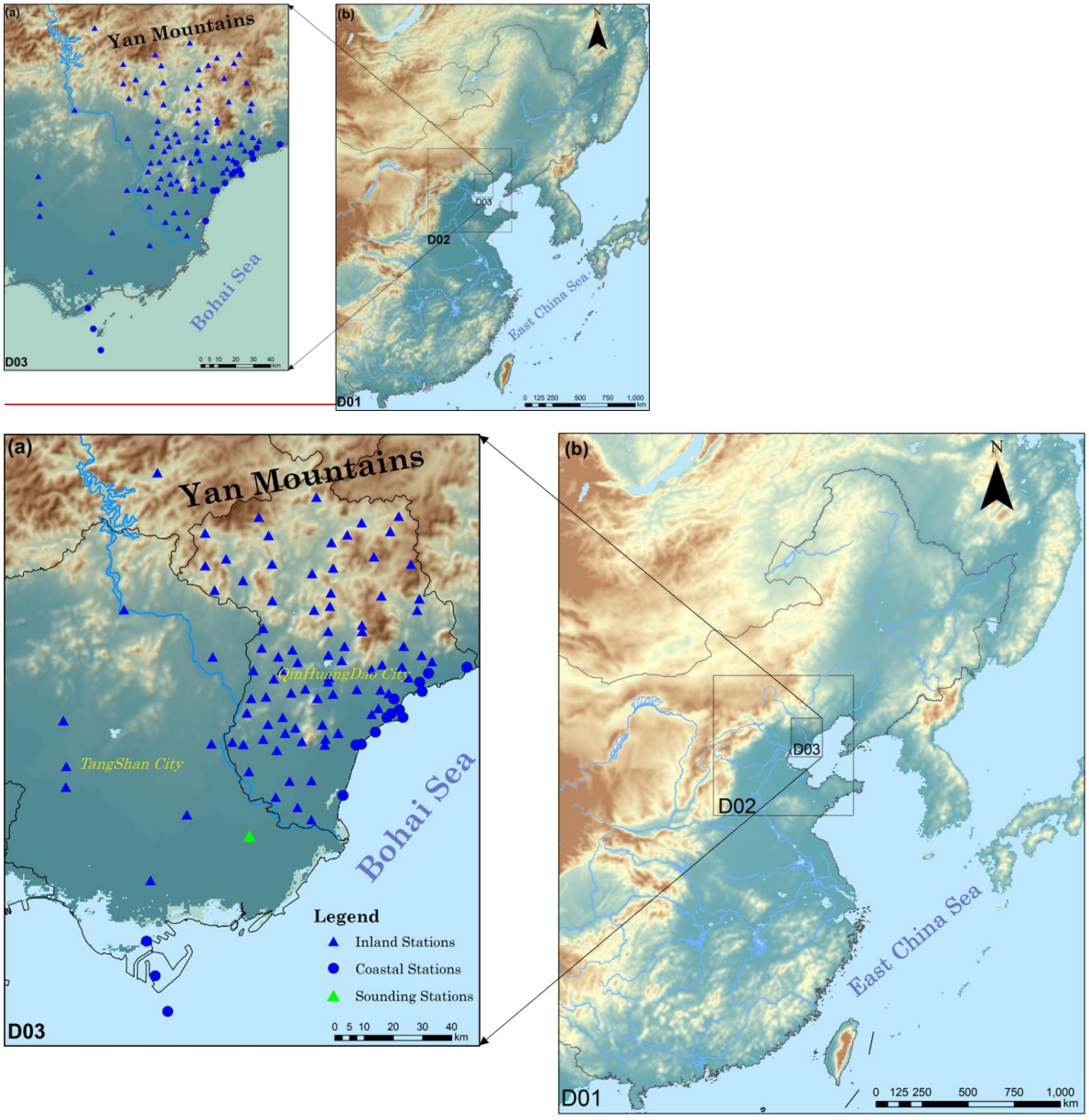

Figure 1: Map showing the (a) study area ~~(a)~~ and (b)WRF nested domains (D01–D03) ~~(b)~~. Solid blue circles and triangles in (a) represent coastal ~~weather stations~~ (16 in total) and inland ~~weather~~ stations (89 in total), and green triangle represent sounding station~~respectively~~.

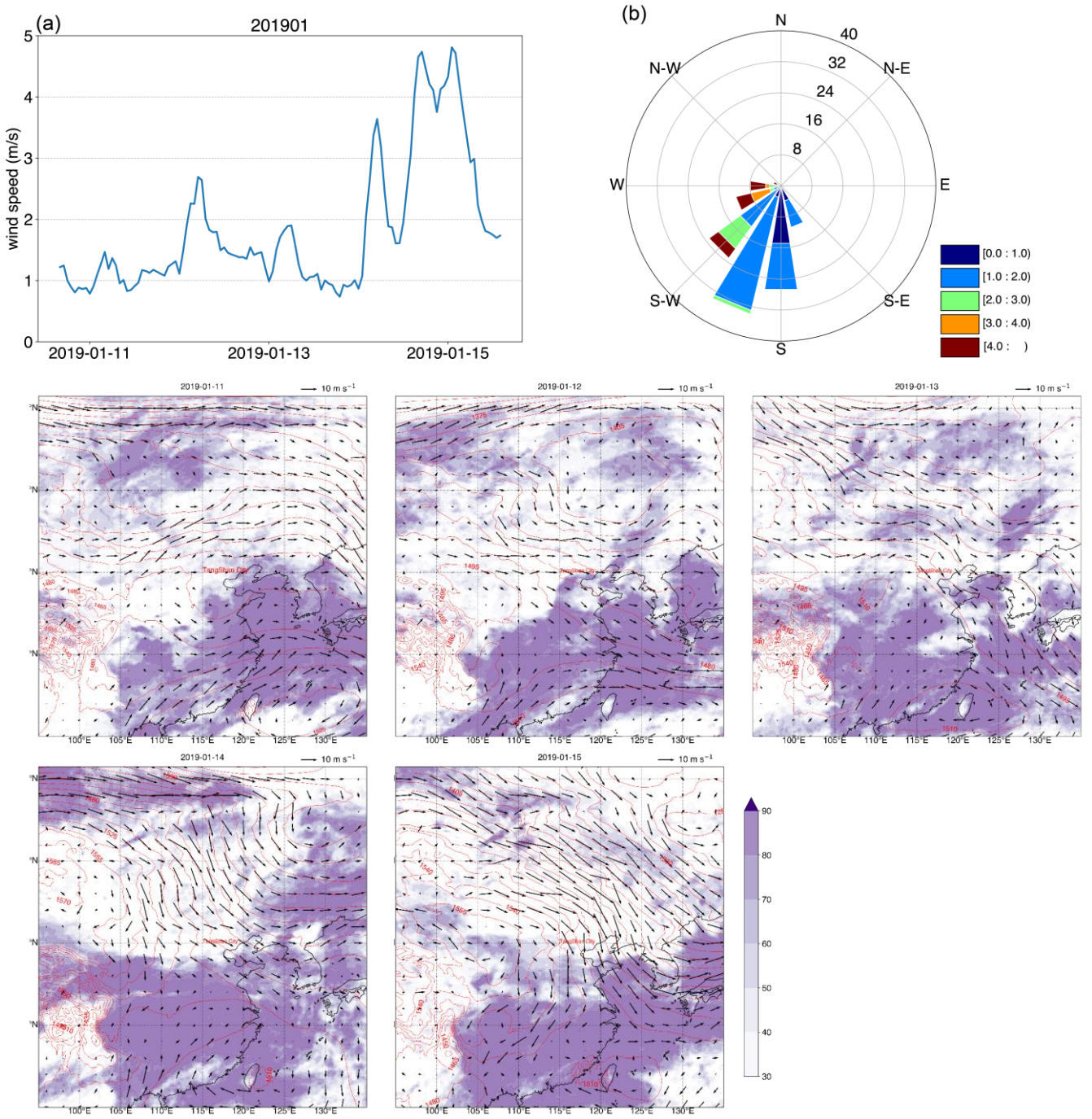

865

Figure 2: The daily averaged geopotential height (contour, units: gpm) , winds (vectors, units: m/s) and cloud fraction (shading, units: %) at 925 hPa during 11 to 15 January 2019.~~Time series of hourly wind speed (a) and the wind rose (b) for January 11th to January 15th, 2019, averaged over the 106 weather stations shown in Figure 1a.~~

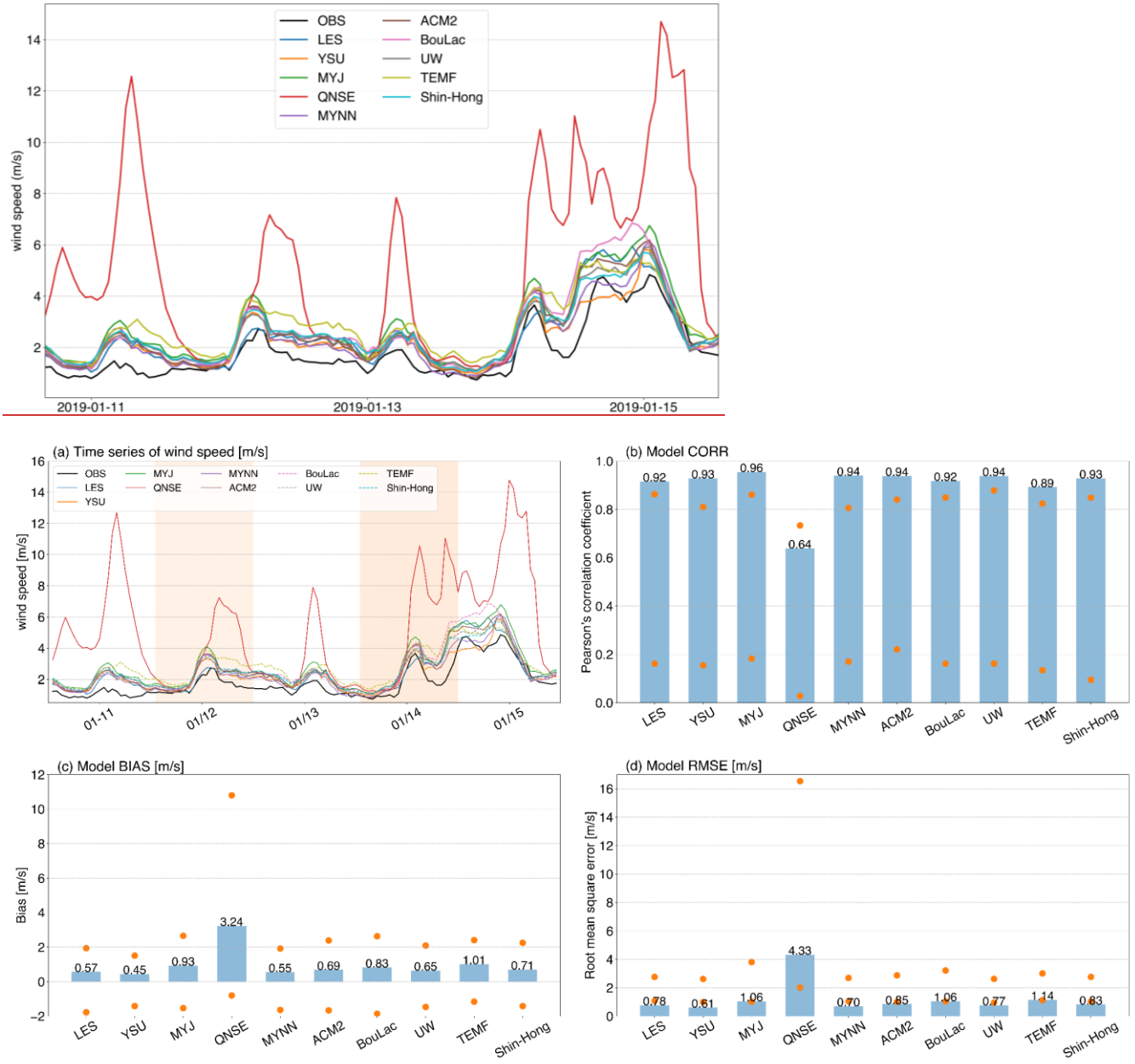

Figure 3: (a) Time series of observed and simulated wind speeds (m/s) and the corresponding statistics of (b) CORR, (c) BIAS and (d) RMSE for the PBL schemes. For each PBL scheme, the average is calculated over the 105 stations and then over all the simulations with that scheme, the dots in b, c and d represent the range across the stations. ~~Time series of observed and simulated wind speeds (m/s) averaged over 106 weather stations. The result for each PBL scheme is the average of all the simulations using that scheme.~~

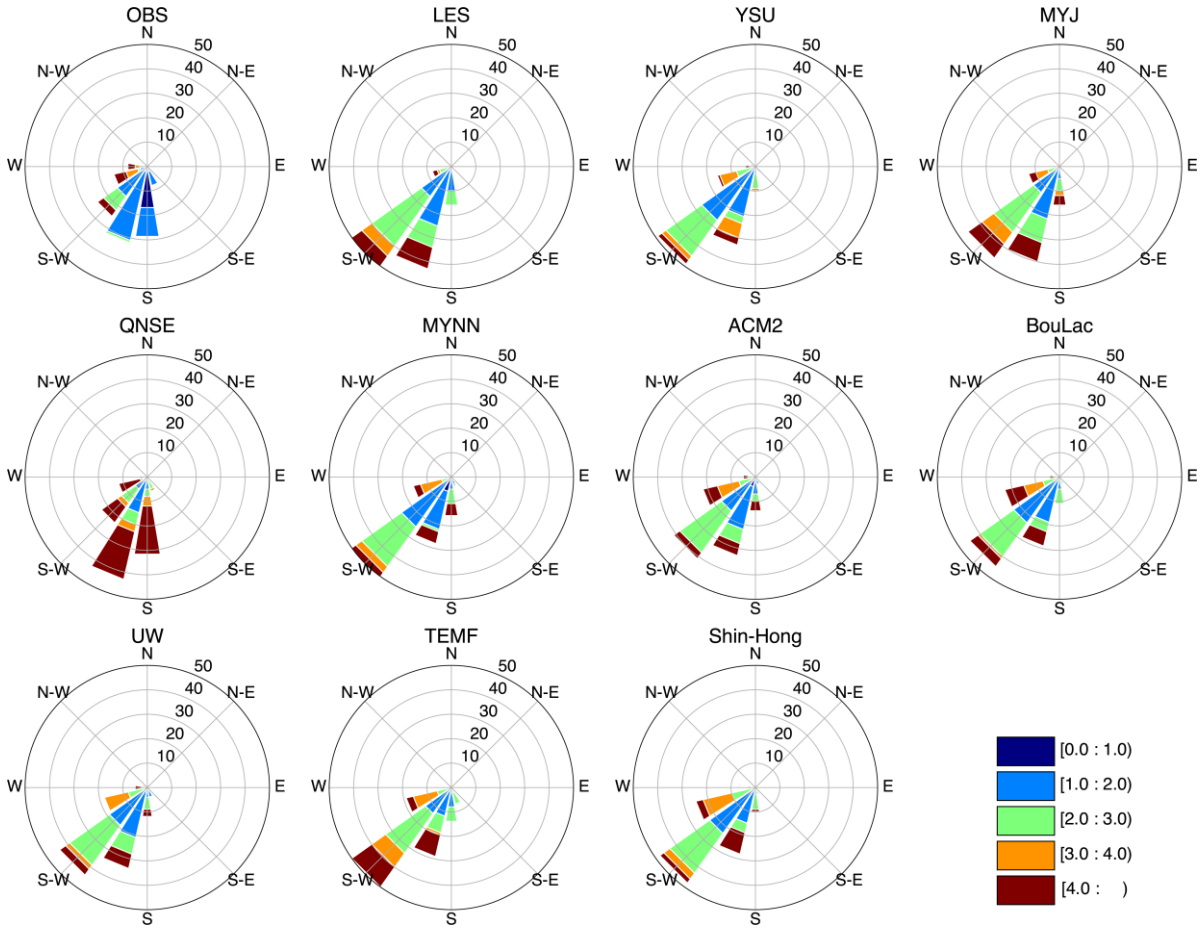
OBS
LES
YSU
MYJ
QNSE
MYNN
ACM2
BouLac
UW
TEMF
Shin-Hong
N
N-E
E
S-E
S
S-W
W
N-W
10
20
30
40
50
[0.0 : 1.0)
[1.0 : 2.0)
[2.0 : 3.0)
[3.0 : 4.0)
[4.0 :)

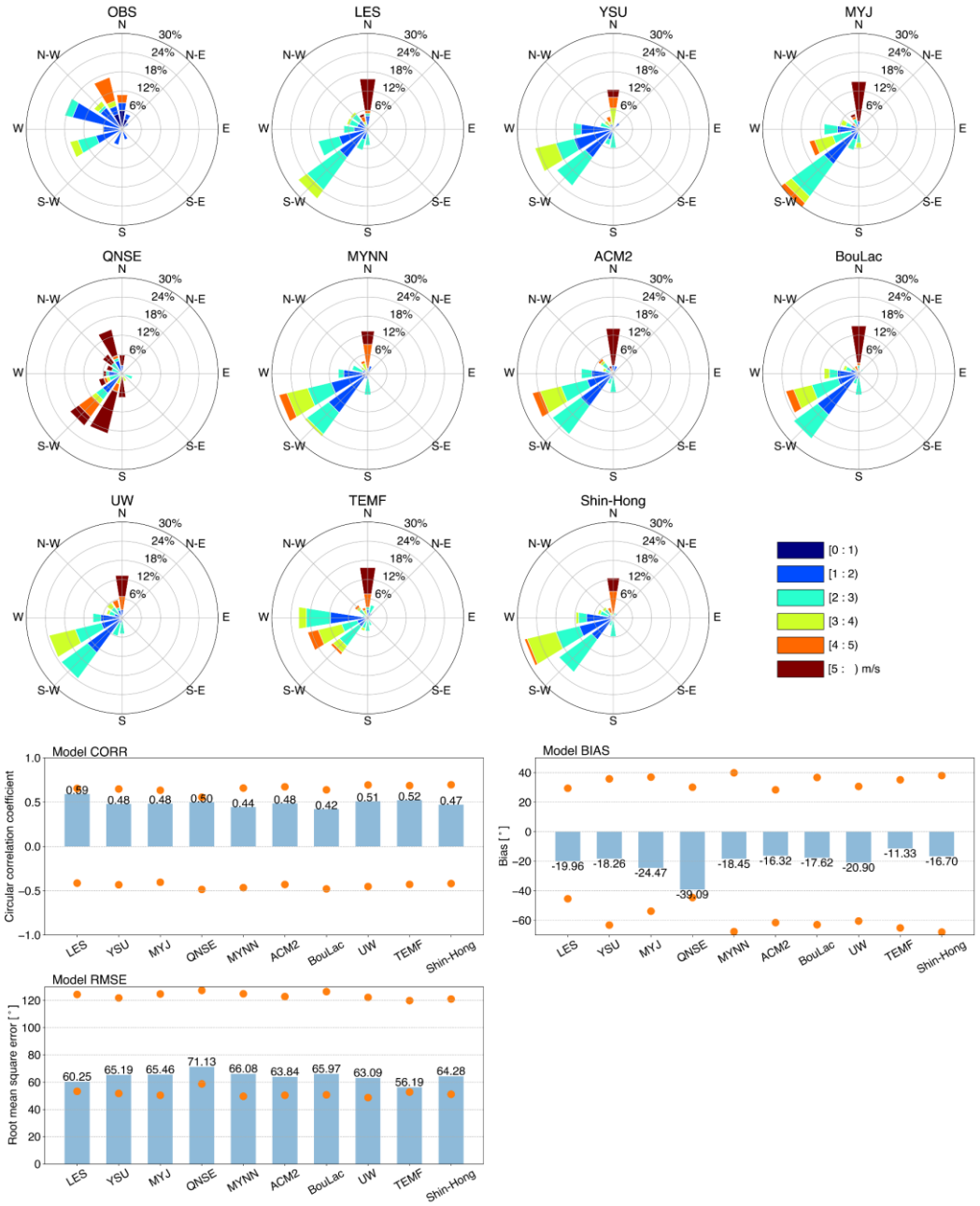

Figure 4: The wind rose charts for the PBL schemes during 11-15 January 2019 averaged over the stations and the corresponding scores of CORR, BIAS and RMSE, for each wind rose chart, the circles represent the relative frequency (%), and the colors represent wind speed (m/s). ~~Wind roses showing observed and simulated differences between PBL schemes.~~

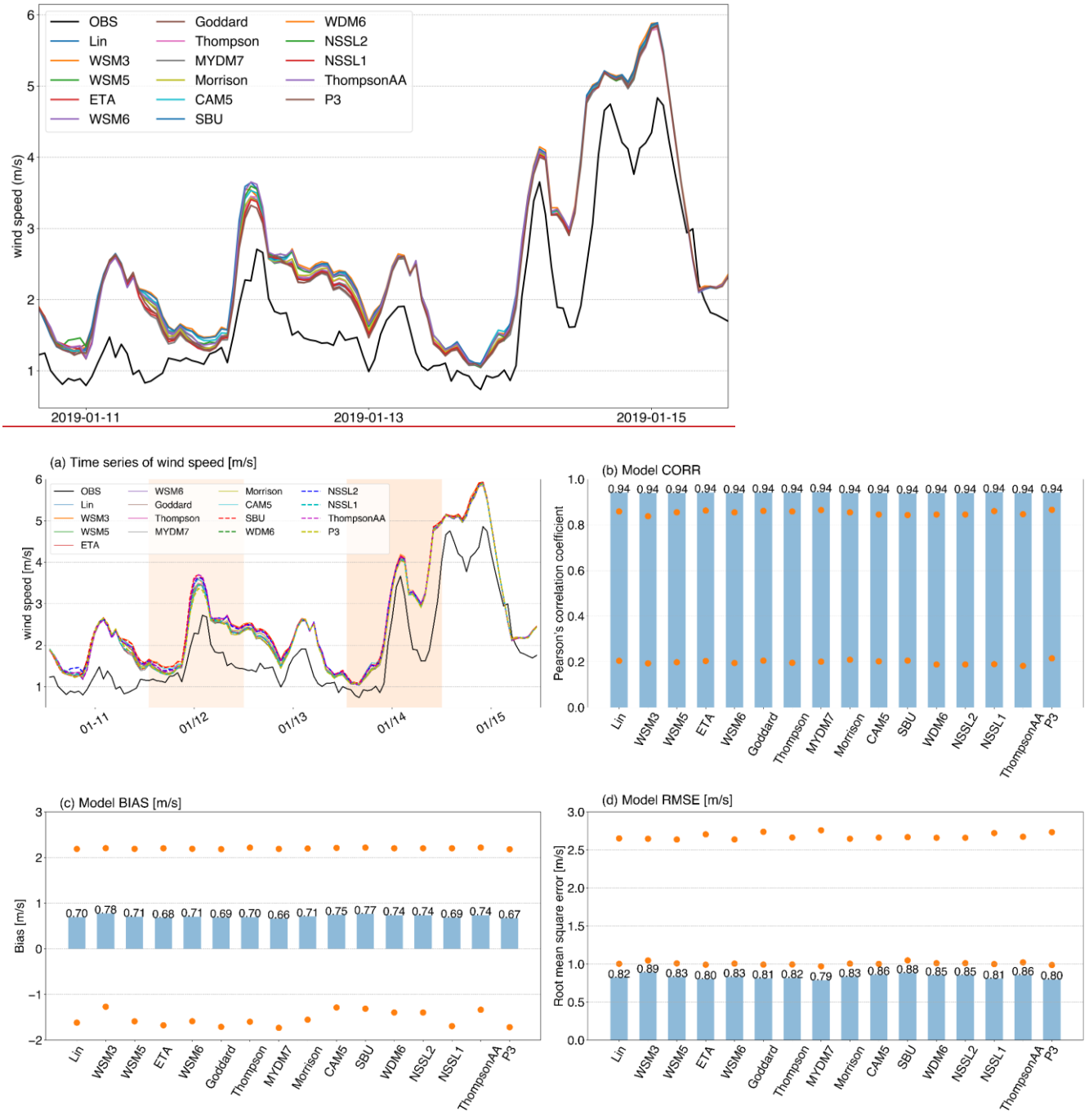

Figure 5: Same as Figure 3, but for MP schemes. ~~Time series for observed and simulated wind speeds (m/s) for different MP schemes.~~

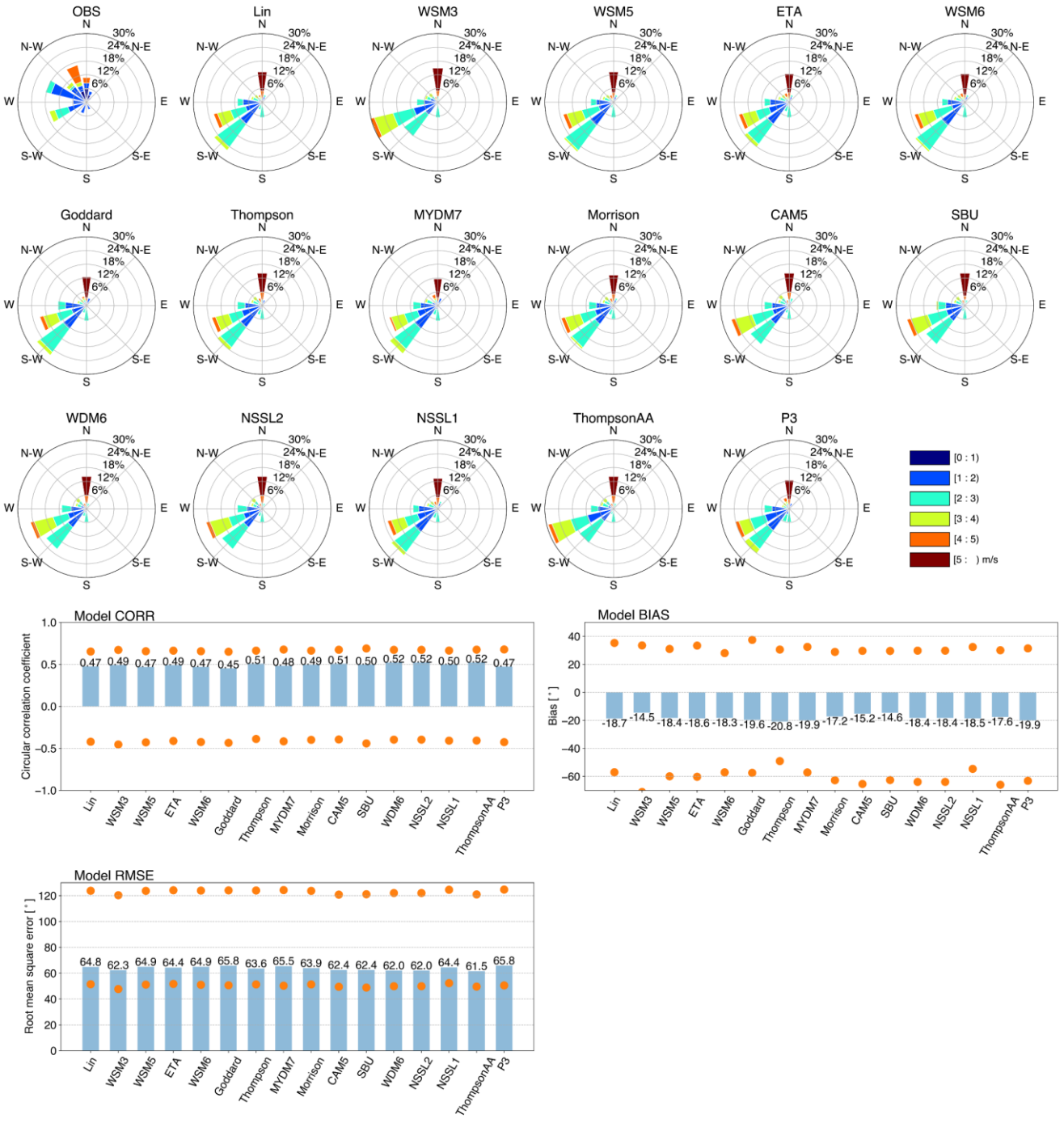

Figure 6: Same as Figure 4, but for MP schemes.

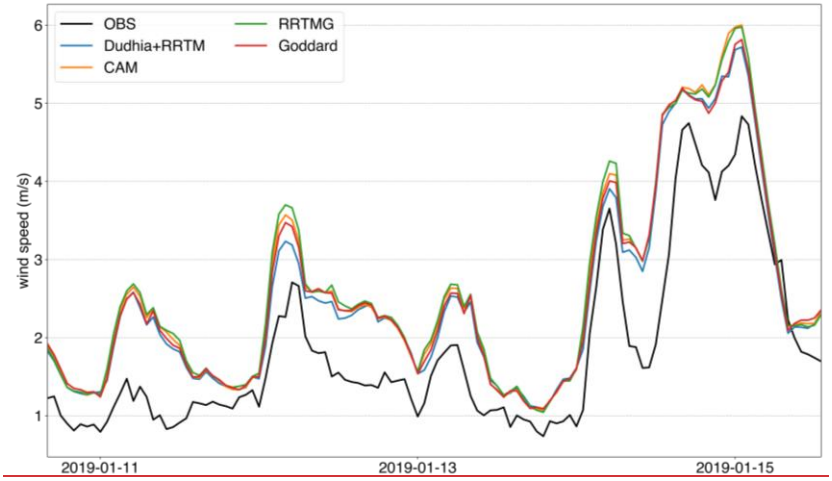

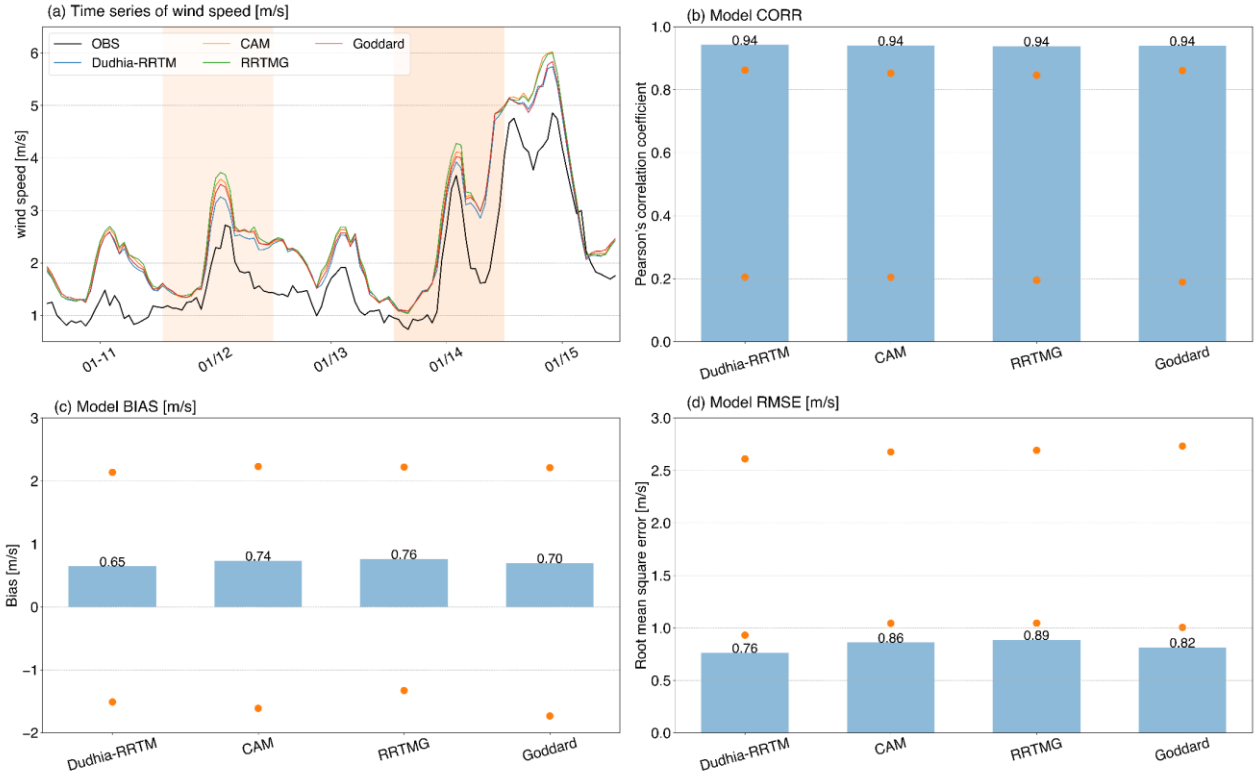

Figure 7: Same as Figure 3, but for SW-LW schemes. ~~6: Time series for observed and simulated wind speeds (m/s) for different LW/SW radiation schemes.~~

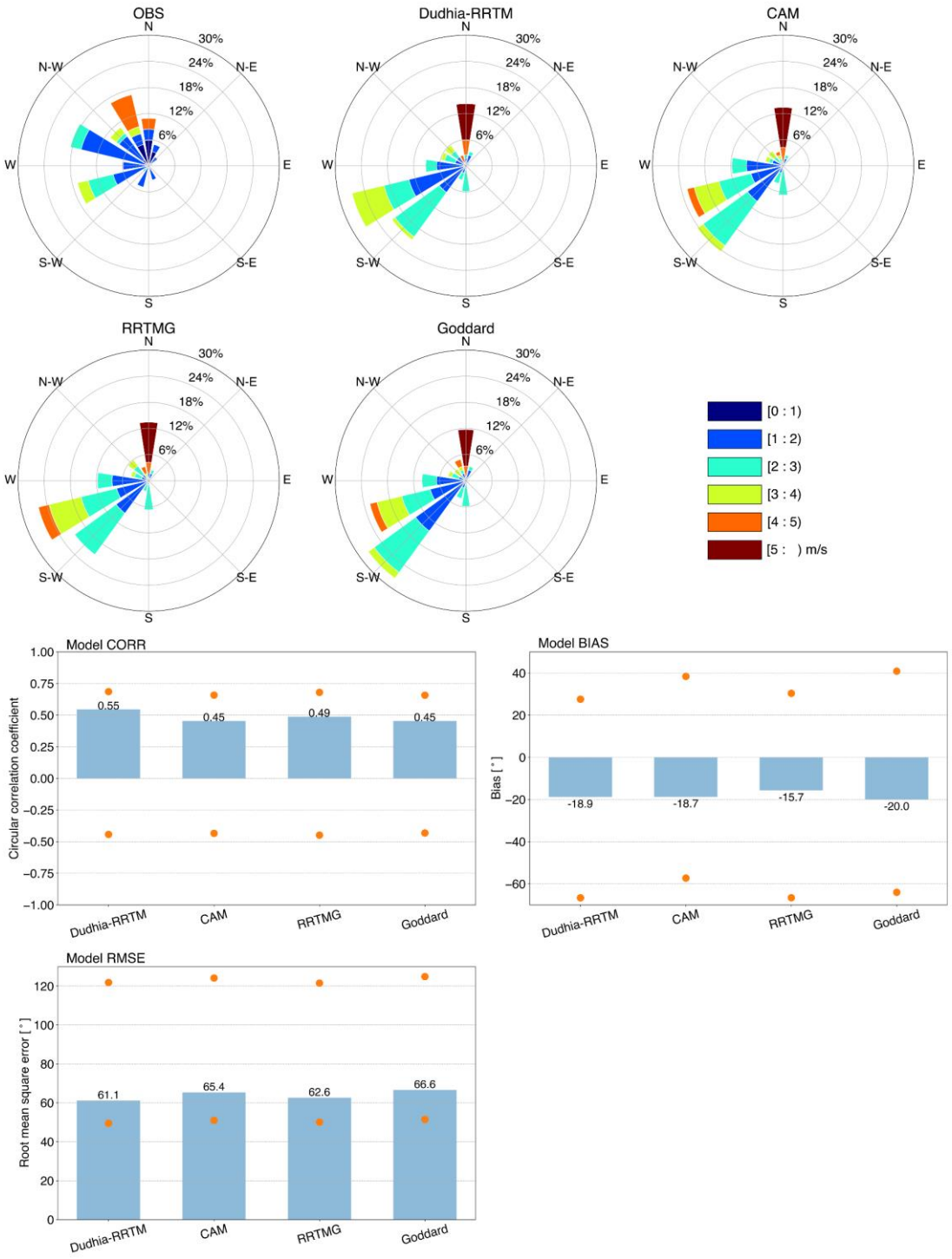

Figure 8: Same as Figure 4, but for SW-LW schemes.

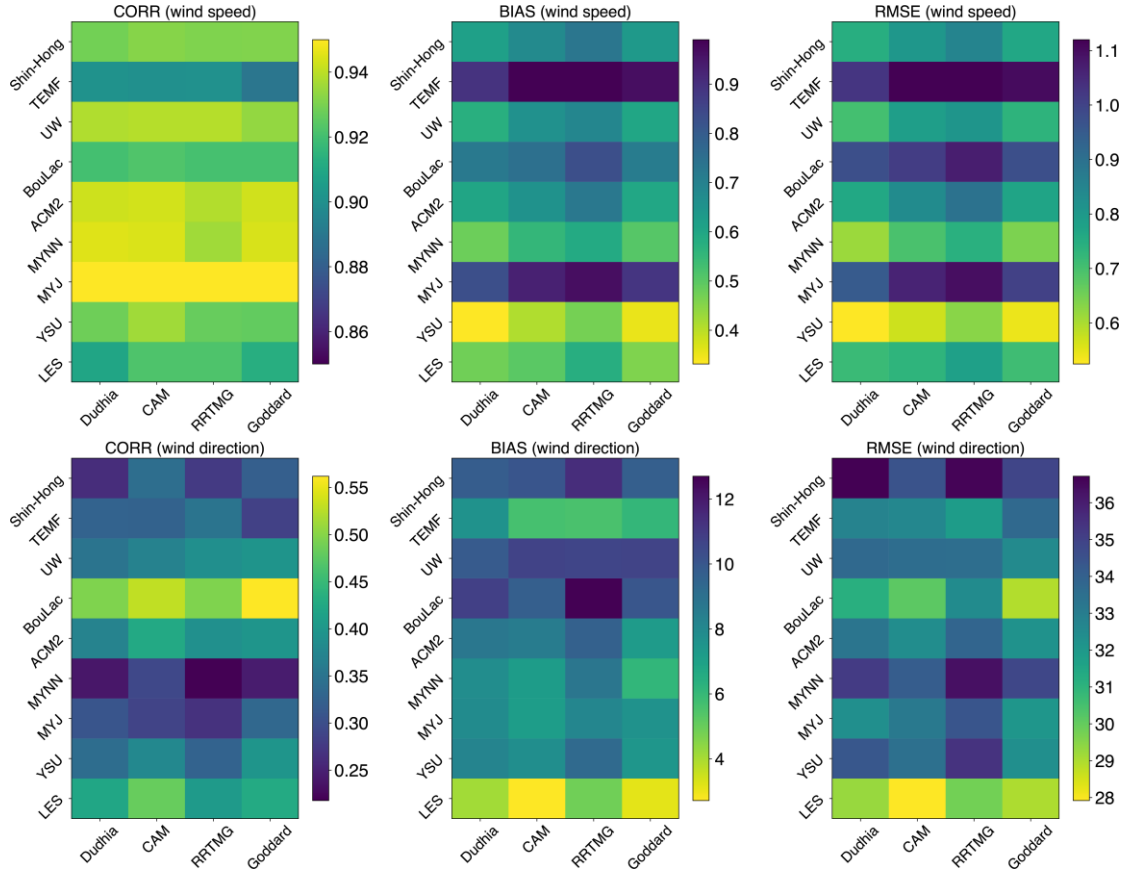
CORR (wind speed)
BIAS (wind speed)
RMSE (wind speed)
CORR (wind direction)
BIAS (wind direction)
RMSE (wind direction)
Shin-Hong
TEMF
UW
BouLac
ACM2
MYNN
MYJ
YSU
LES
Dudhia
CAM
RRTMG
Goddard
0.94
0.92
0.90
0.88
0.86
0.9
0.8
0.7
0.6
0.5
0.4
1.1
1.0
0.9
0.8
0.7
0.6
0.55
0.50
0.45
0.40
0.35
0.30
0.25
12
10
8
6
4
36
35
34
33
32
31
30
29
28

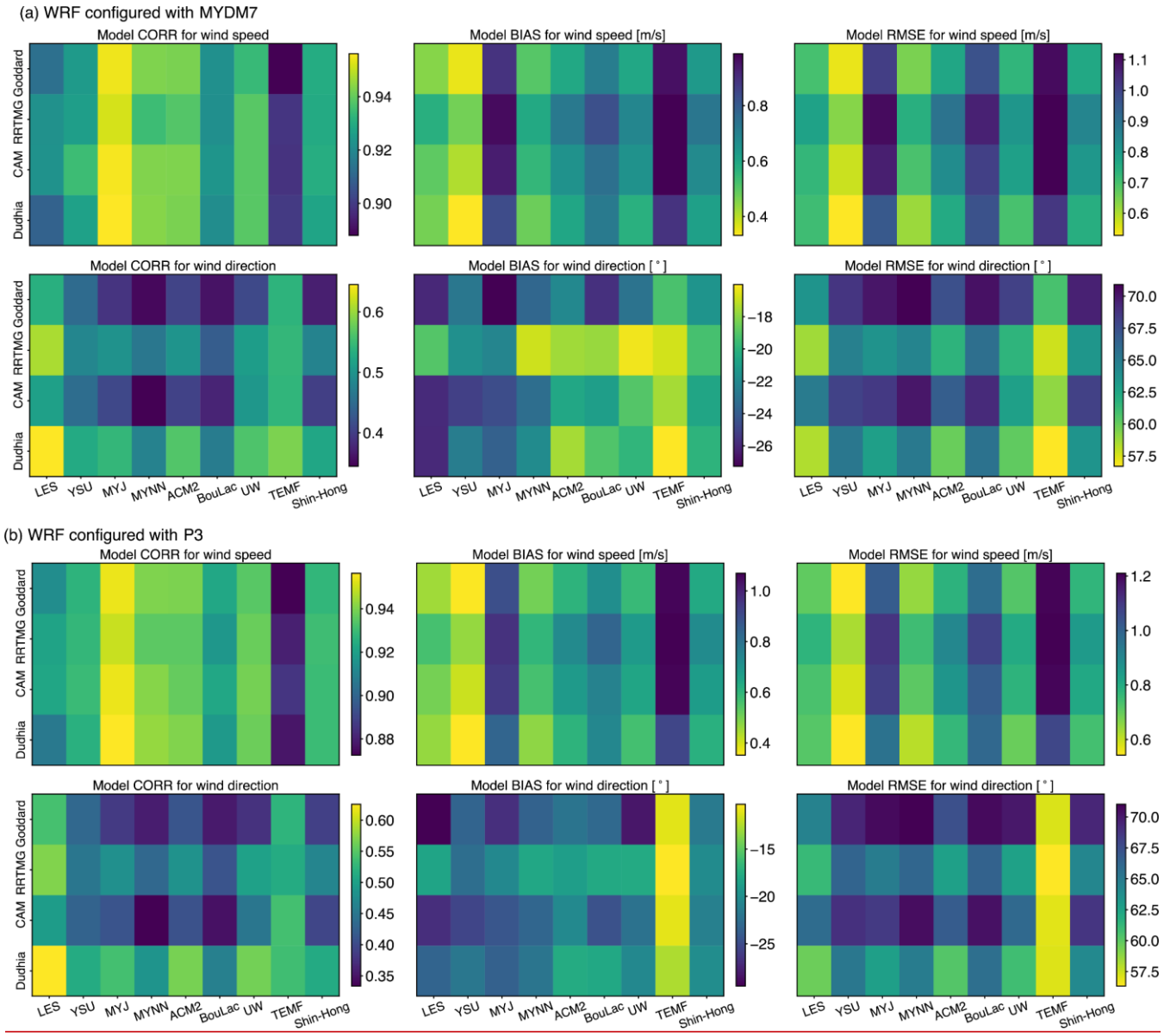

Figure ~~97~~: Statistic scores (CORR, BIAS and RMSE) for wind speed ~~(upper panels)~~ and direction ~~(lower panels)~~ for different combinations of PBL and LW ~~/~~SW ~~radiation~~ schemes. The MP scheme used is~~was~~ MYDM7 and P3.

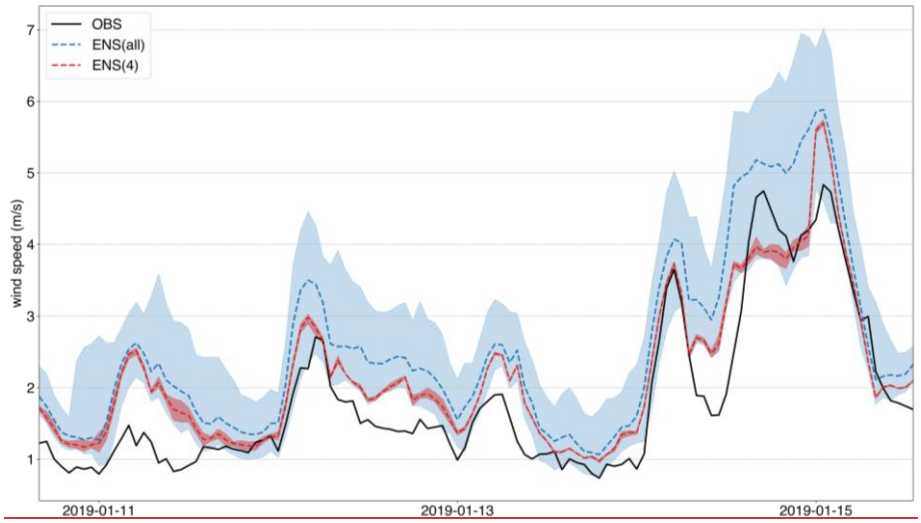

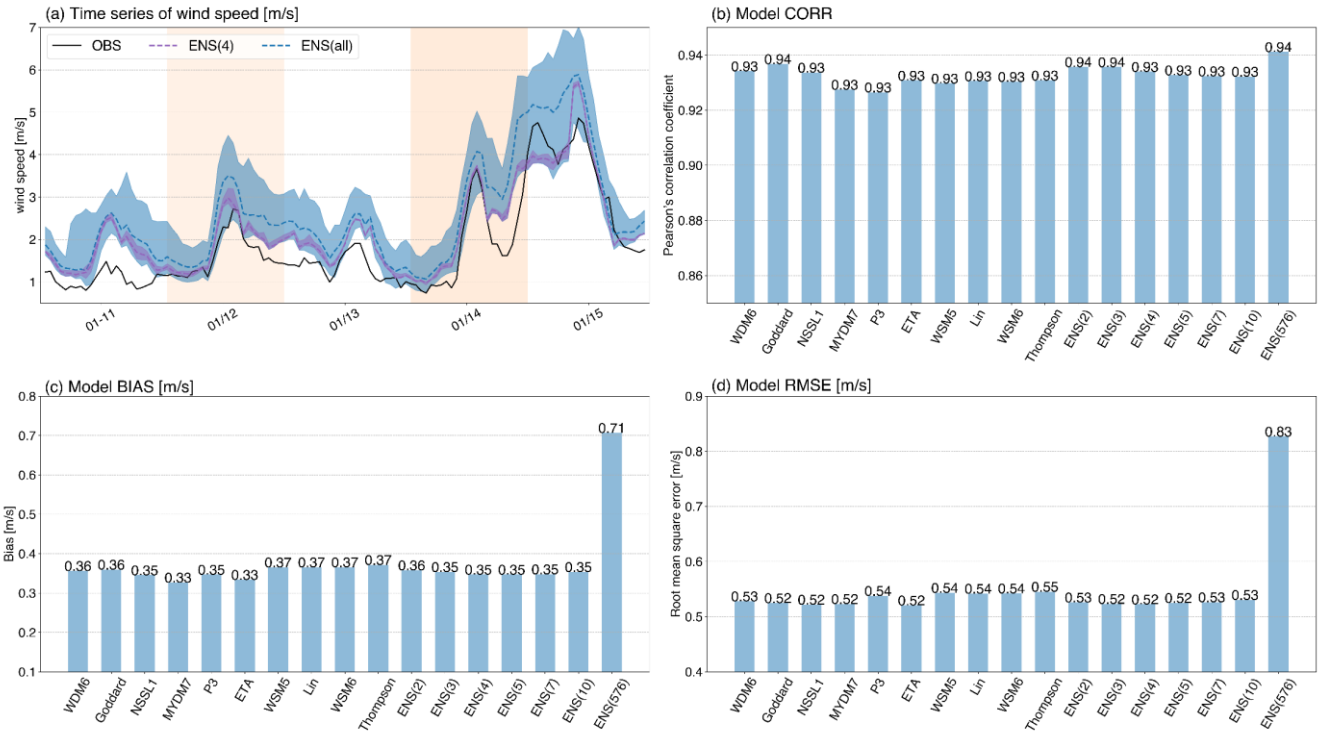

Figure 108: (a)Time series of wind speed (m/s) from observations and different ensembles, ~~including an ensemble of the top four schemes and an ensemble of all the simulations. S~~ shading shows the spread, and the corresponding CORR, BIAS and RMSE scores are shown in b-d. ~~of the corresponding simulations.~~

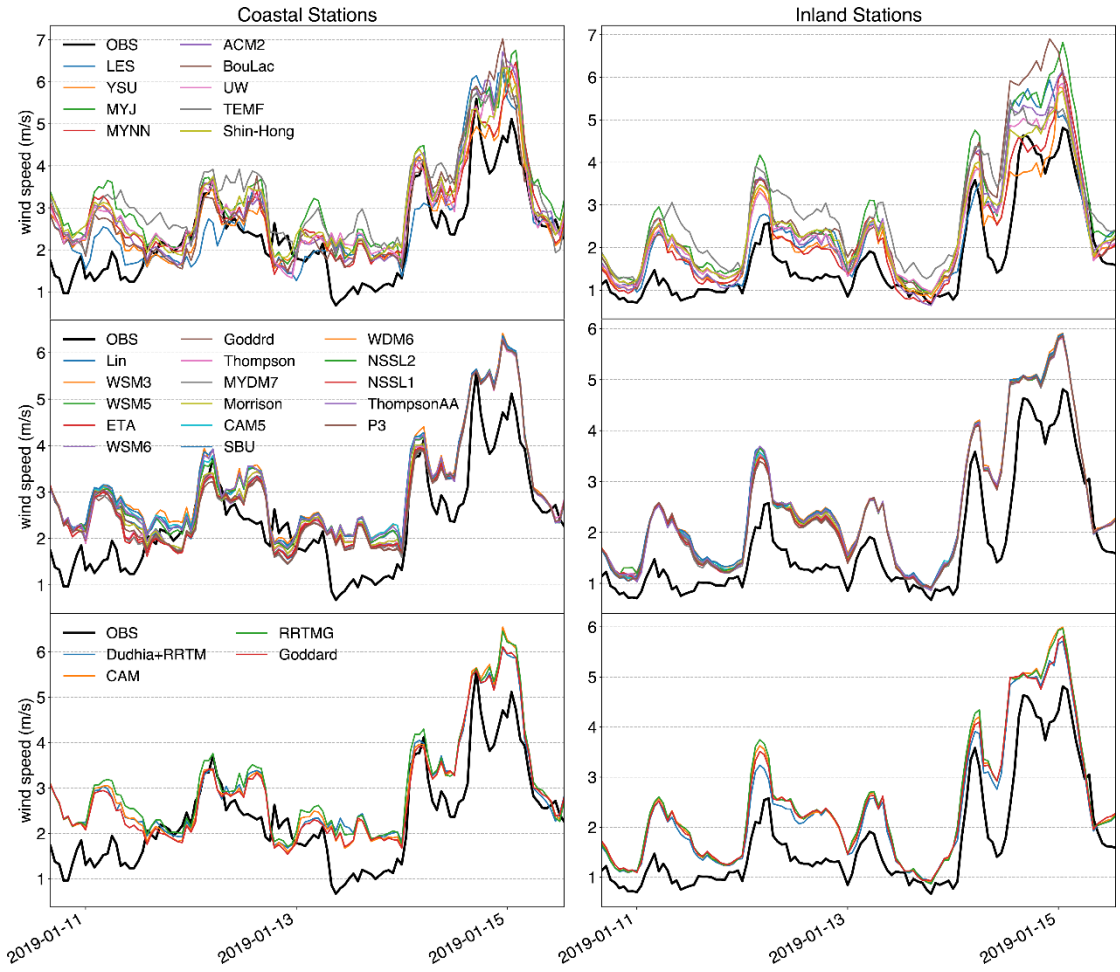
Coastal Stations
Inland Stations
wind speed (m/s)
OBS
LES
YSU
MYJ
MYNN
ACM2
BouLac
UW
TEMF
Shin-Hong
OBS
Lin
WSM3
WSM5
ETA
WSM6
Goddrd
Thompson
MYDM7
Morrison
CAM5
SBU
WDM6
NSSL2
NSSL1
ThompsonAA
P3
OBS
Dudhia+RRTM
CAM
RRTMG
Goddard
2019-01-11
2019-01-13
2019-01-15

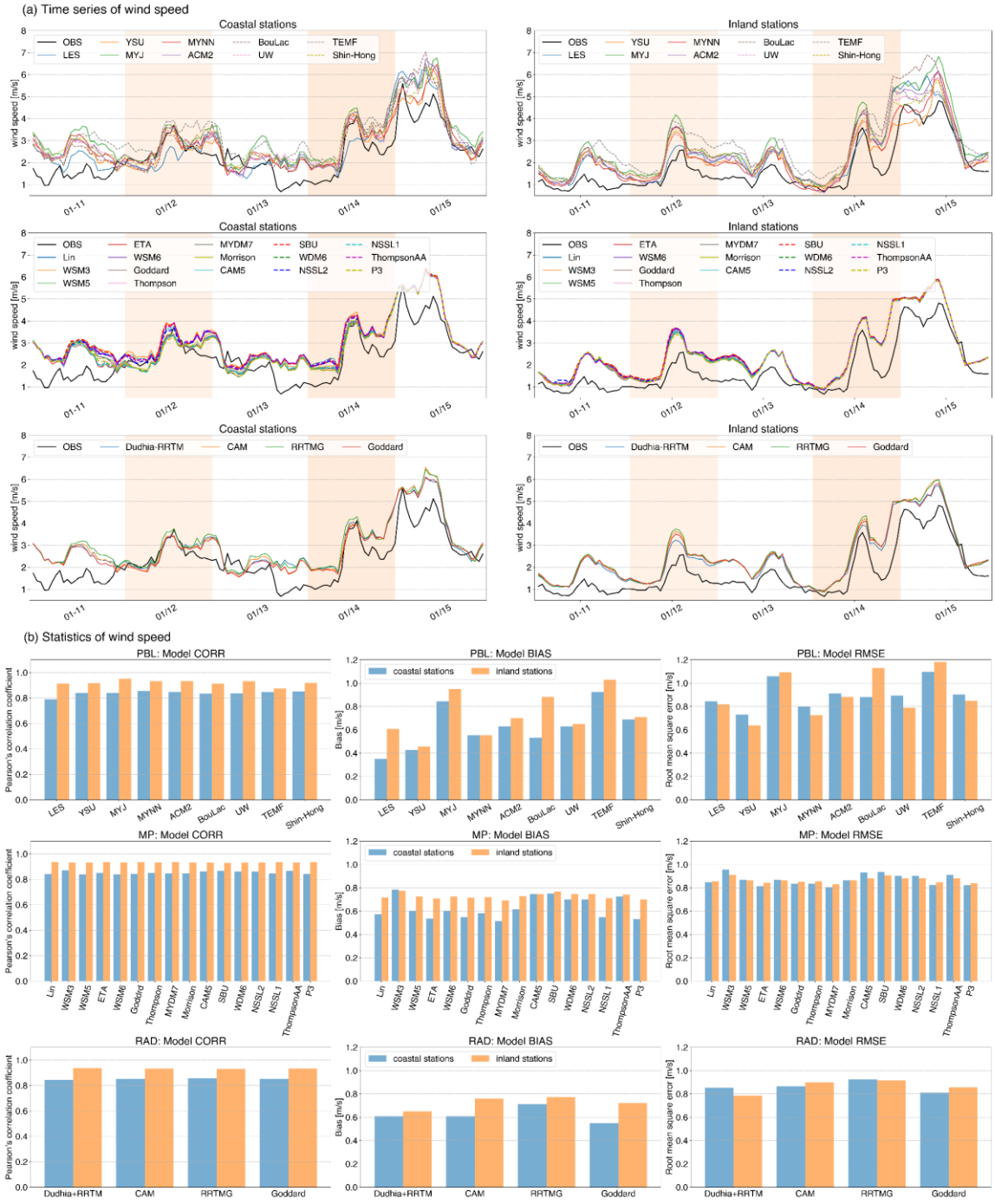

910 **Figure 119: Comparison of simulated wind speeds between the coastal ~~(left)~~ (89 in total) and inland ~~(right)~~(16 in total) stations shown in Figure 1a, as well as the corresponding statistic scores.**

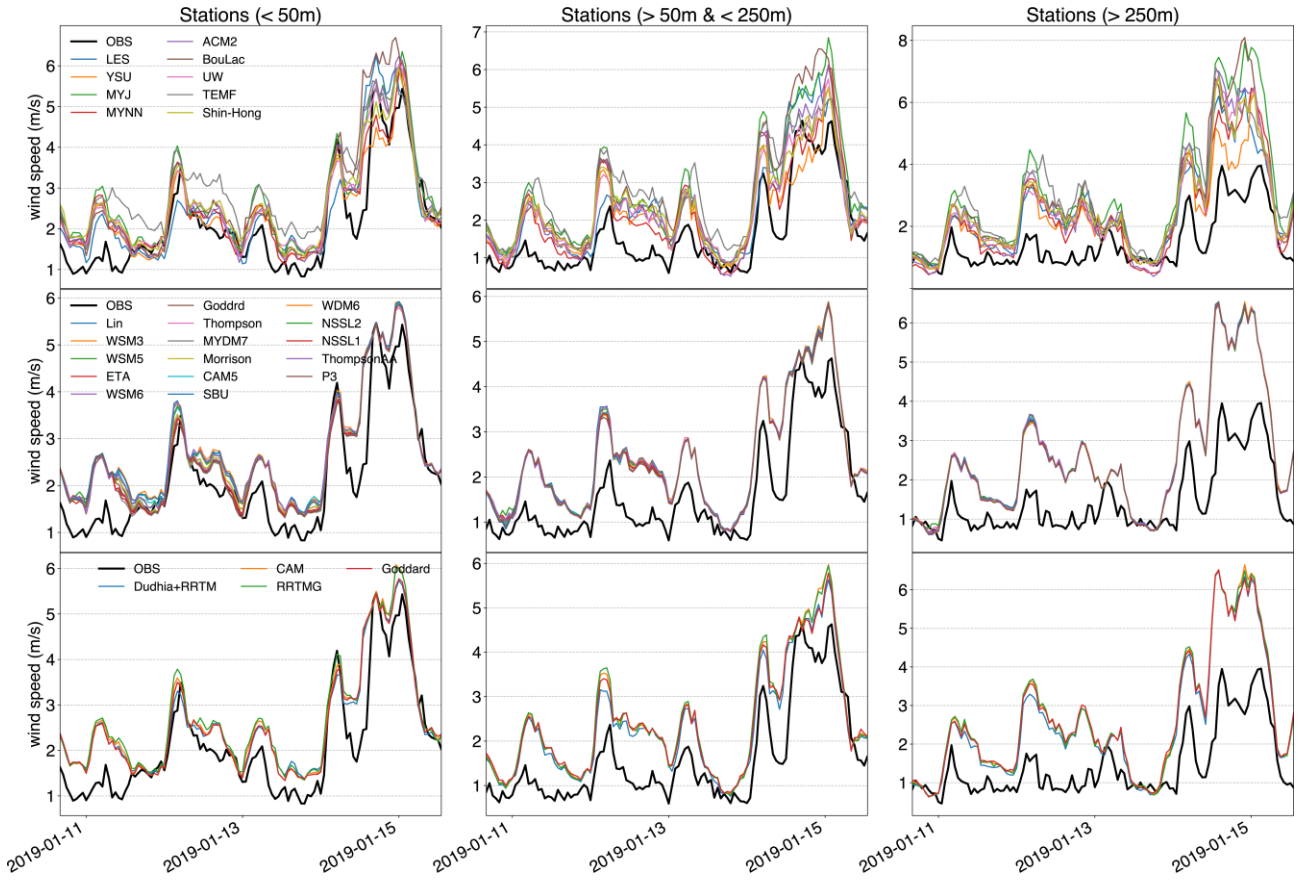
Stations (< 50m)
Stations (> 50m & < 250m)
Stations (> 250m)
wind speed (m/s)
OBS
LES
YSU
MYJ
MYNN
ACM2
BouLac
UW
TEMF
Shin-Hong
OBS
Lin
WSM3
WSM5
ETA
WSM6
Goddrd
Thompson
MYDM7
Morrison
CAM5
SBU
WDM6
NSSL2
NSSL1
Thompsonaer
P3
OBS
Dudhia+RRTM
CAM
RRTMG
Goddard
2019-01-11
2019-01-13
2019-01-15

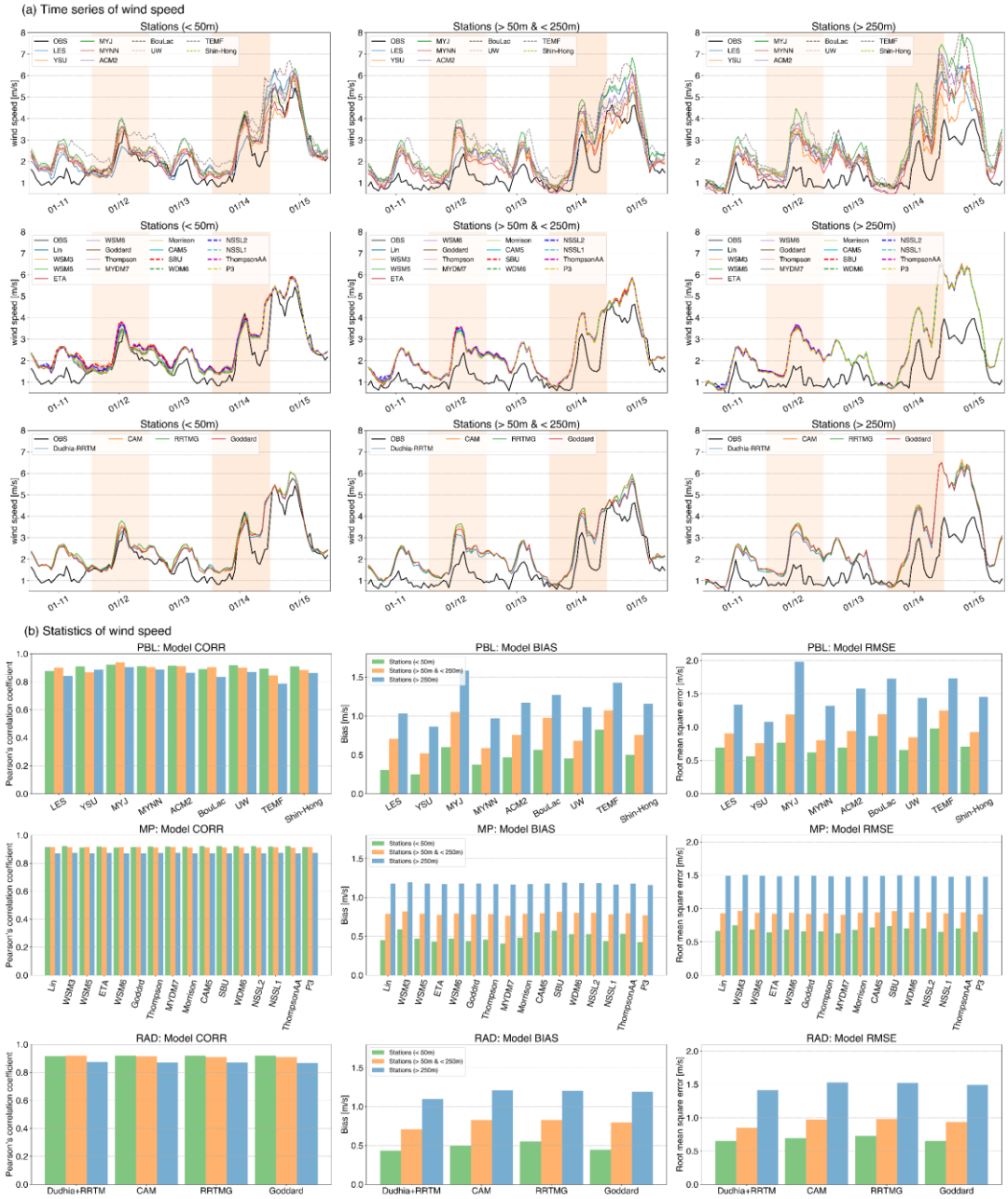

Figure 1<u>2</u>~~0~~: Comparison of simulated wind speeds (m/s) for stations <u>< 50m (51 in total), >50 & < 250m (36 in total) and < 250m (19 in total) and the corresponding statistic scores.</u> ~~located at different altitudes.~~

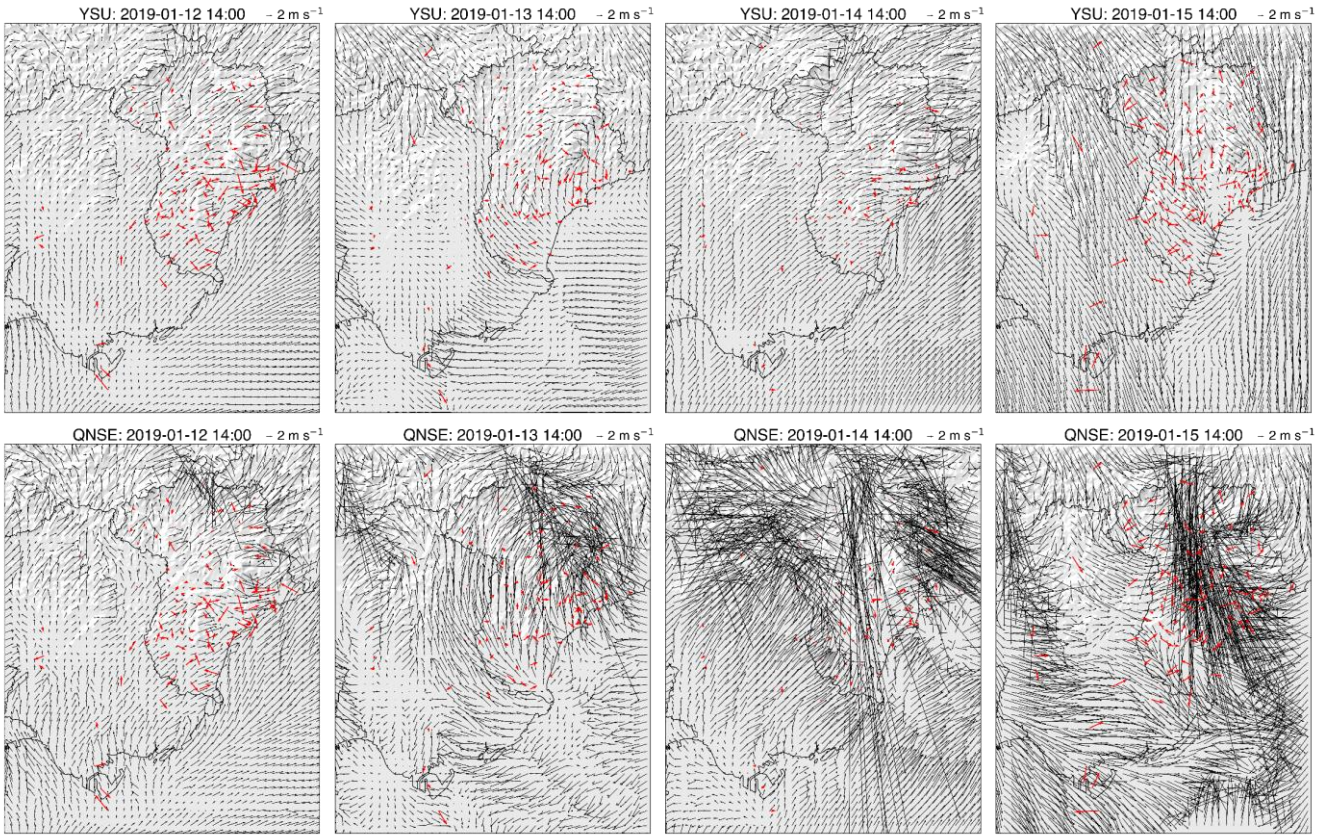

Figure 13: Spatial distribution of simulated (black vector) and observed (red vector) winds at 14:00 (local time) during the study period from simulations with the YSU and QNSE schemes.

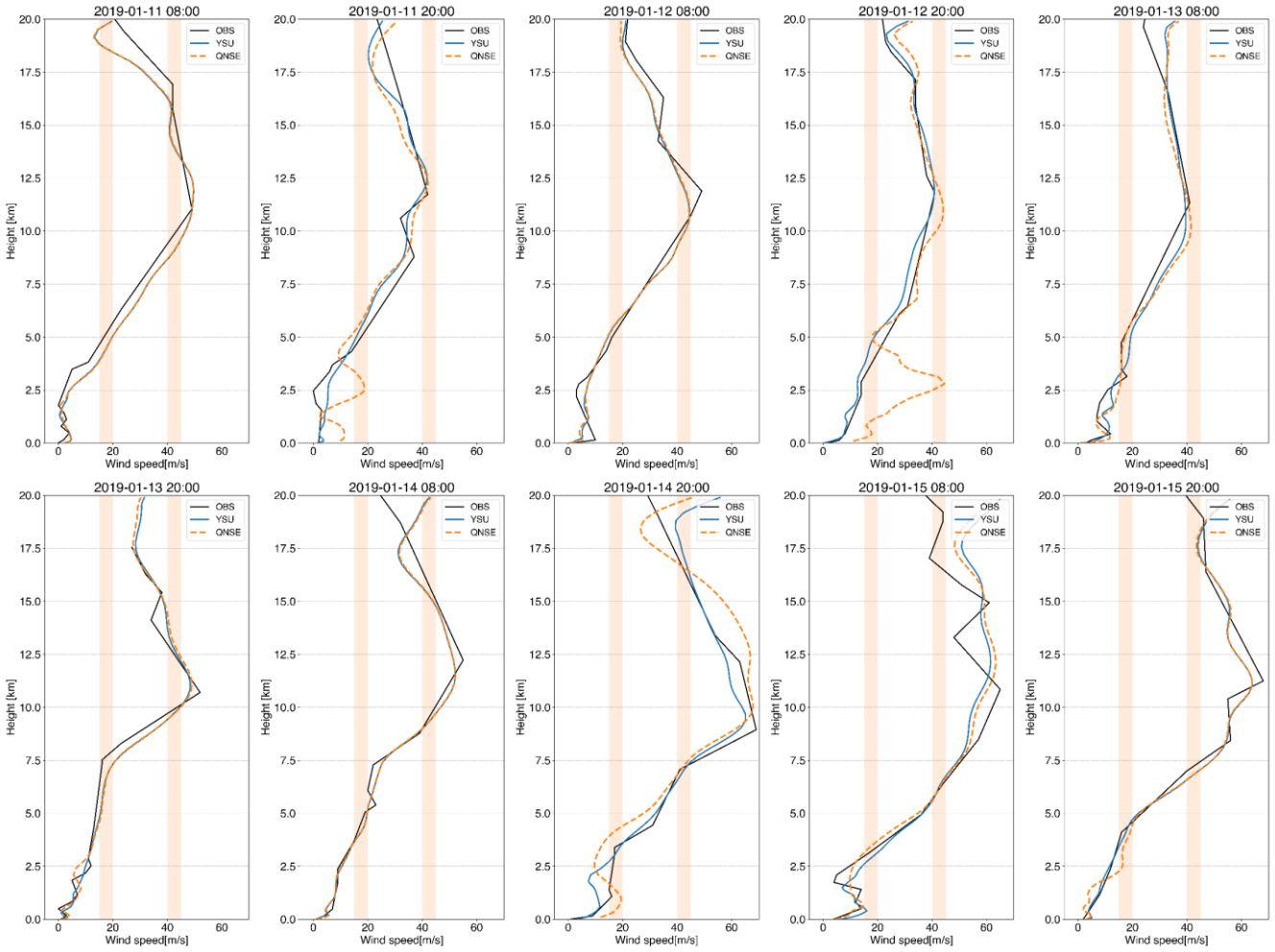

Figure14: Wind speed profile from observation and simulations with the YSU and QNSE schemes at 08:00 and 20:00 (local time) during the study period.

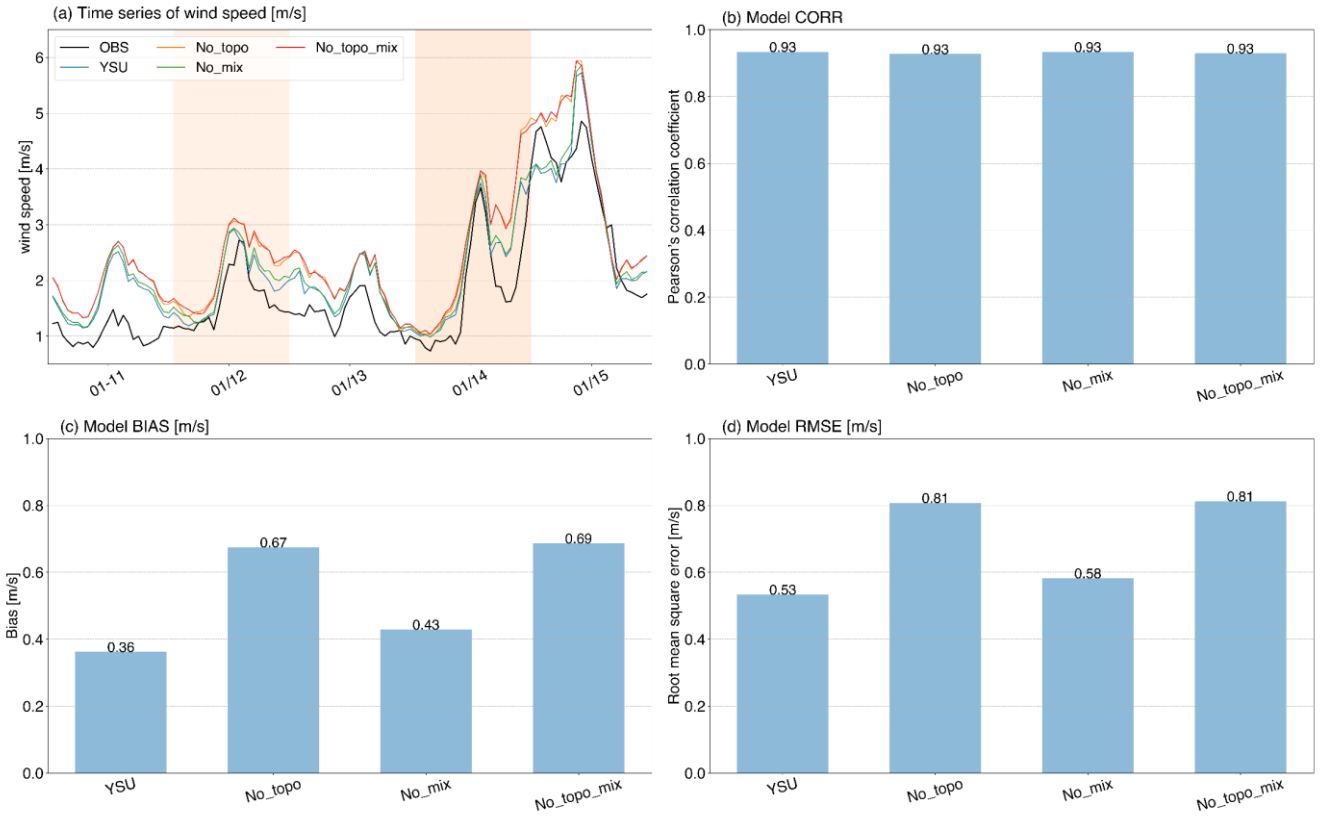

Figure 15: Same as Figure 3, but for simulations with different YSU options.

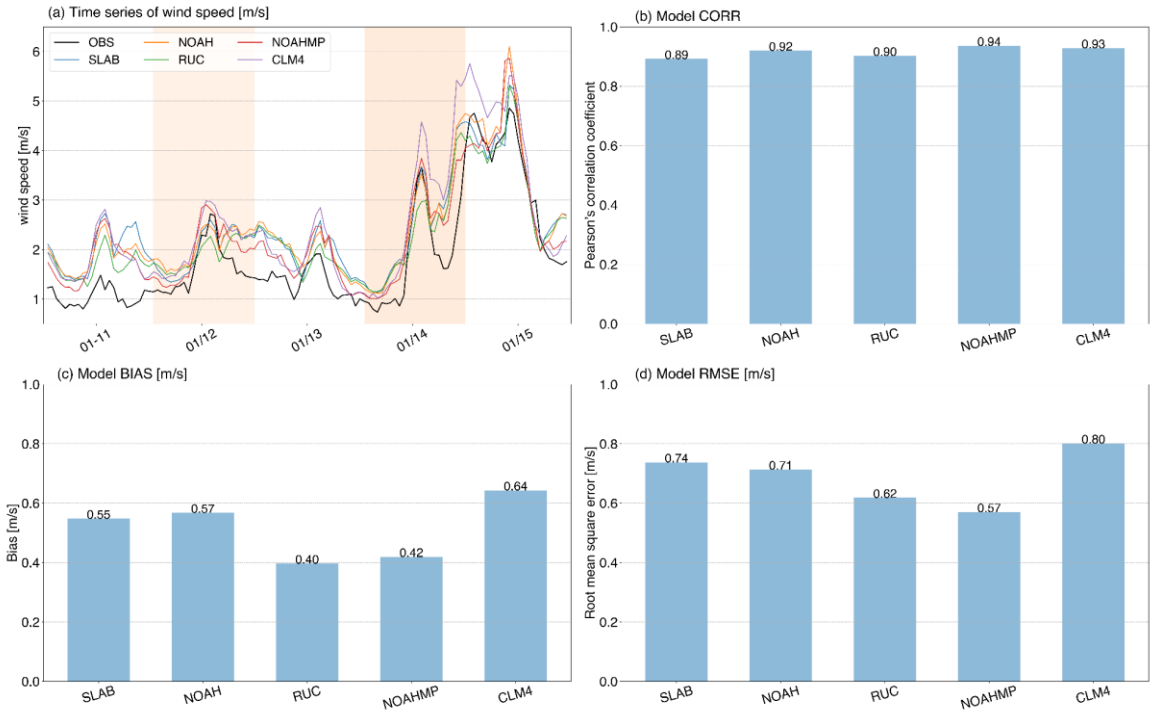

Figure 16: Same as Figure 3, but for simulations with different land surface schemes.